FINAL REPORT

Detecting events and seasonal trends in biomass burning plumes using black and brown carbon: $(BC)^2$ El Paso

AQRP Project Number: **19-031**

Prepared for

Texas Air Quality Research Program (AQRP)
The University of Texas at Austin

Prepared by
Rebecca Sheesley (Principal Investigator)
Baylor University

Sascha Usenko
Baylor University

James Flynn
University of Houston

September 2019

QA Requirements: Audits of Data Quality: 10% Required

ACKNOWLEDGMENT

The preparation of this report is based on work supported by the State of Texas through the Air Quality Research Program administered by The University of Texas at Austin by means of a Grant from the Texas Commission on Environmental Quality. The findings, opinions and conclusions are the work of the author(s) and do not necessarily represent findings, opinions, or conclusions of the AQRP or the TCEQ.

Executive Summary

Recent efforts by Texas Air Quality Research Program (AQRP) and TCEQ to monitor and study air quality in Texas cities has resulted in improved understanding of the processes and sources which control urban air quality in e.g. Houston. As highlighted in the AQRP Priority Research Areas 2018-2019, El Paso is near the National Ambient Air Quality Standards for particulate matter (PM) and ozone (O_3). Reductions in anthropogenic emissions through the implementation of cleaner technologies for e.g. motor vehicle exhaust, coal-fired power plants, have refocused efforts to understand the contribution of biomass burning to urban air pollution. This is particularly relevant for El Paso, which can experience large impacts of periodic biomass burning/wildfire plumes transported from out-of-state. Black carbon (BC), a marker for combustion influences on air quality, has been shown to be decreasing in urban areas across the United States due to increased regulation and the use of cleaner fuels (Kirchstetter et al. 2017). As a result, biomass burning contributions are likely becoming more important for BC and for urban air quality in general.

This project has provided critical new a methodology to ascertain the influence of biomass burning on air quality in El Paso, TX through the characterization of BC and brown carbon (BrC). BrC is the carbon fraction of an aerosol that selectively absorbs short wavelengths of light (i.e. ultraviolet or UV). Influence of biomass burning plumes was identified using aerosol optical properties, including aerosol light absorption and scattering coefficients for specific UV and visible wavelengths combined with absorption Ångström exponents (AAE) and scattering Ångström exponents (SAE) (Sandradewi et al. 2008b, Laing et al. 2016). When light absorption by atmospheric aerosols is dominated by BrC rather than BC, such as when there is increased influence from biomass burning on aerosols, the AAE is much greater than one. When the aerosol absorption is dominated by BC, like in motor vehicle exhaust, the AAE is close to one. The newest technology for real-time monitoring of aerosol absorption is the tricolor absorption photometer (TAP). The TAP measures absorption at UV, green and red wavelengths to more specifically target this biomass burning influence. This inexpensive and continuous photometer was designed by National Oceanic and Atmospheric Administration (NOAA) and is commercially produced by Brechtel to address issues with previous photometers, including cost, sensitivity, noise and, effective scattering corrections

(Ogren et al. 2017). Light extinction by atmospheric aerosols includes both absorbing and scattering components. Both absorption and scattering coefficients have potential to be used to classify biomass burning, combustion and dust impacts of urban air quality. Since Texas cities are periodically impacted by all these sources, a combined absorption and scattering monitoring approach, similar to that used by NOAA and the Department of Energy, was implemented for $(BC)^2$ El Paso. The two goals of $(BC)^2$ El Paso are to 1) address scientific air quality questions of frequency, seasonality, and optical properties of biomass burning plumes in El Paso and 2) to evaluate the TAP instrument suite for application in long-term monitoring at urban sites in Texas.

The PIs conducted a multi-month field deployment of two TAPs, a seven-channel aethelometer (Magee Scientific AE42), and a three-wavelength nephelometer (TSI 3563) to characterize aerosol optical properties, including multi-wavelength light absorption and scattering during $(BC)^2$ El Paso. Measurements of light absorption and scattering coefficients and the calculated AAE and SAE were used in a proof-of-concept study to identify when biomass burning influenced El Paso air quality during the Mar-Jun 2019 campaign. The aerosol optical properties were also used to identify dust events. In addition to these aerosol optical property measurements, trace gas, satellite fire data and back trajectories were used to further support classification and extent of biomass burning influence. This suite of aerosol and trace gas instrumentation was installed in the Baylor Air Quality Trailer, which was deployed on a newly constructed pad adjacent to the TCEQ CAMS 12 (UTEP) air monitoring site and managed remotely by the Baylor-UH team.

Major Findings

1. The TAP + nephelometer was used to identify influence of biomass burning events on El Paso air quality. Findings were supported using satellite fire products and back trajectories.
2. For seasonality during $(BC)^2$ El Paso in 2019, June was identified to have the most influence from biomass burning, while April-May had the most influence from dust events.
3. The use of AAE allowed for BB events to be identified, even in a complex urban atmosphere when changes in concentration alone are not indicative.

4. The TAP + nephelometer instrument suite provided a relatively low maintenance solution to conducting a long-term BB monitoring campaign.

Recommendations for Future Analysis

1). Conduct a $(BC)^2$ Houston scientific study to investigate the influence of BB in Houston, TX.

2). Analyze co-located $PM_{2.5}$ filters for radiocarbon and potassium ion to quantify the impact of biomass burning on $PM_{2.5}$ concentrations and to establish relationships between changes in AAE and contribution of biomass burning.

3). Couple aerosol optical depth and modeling with $(BC)^2$ study to understand transport and potential influence on ozone or other air quality parameters.

4) Target June in El Paso for future, intensive measurement campaigns for detailed volatile organic compounds (VOCs), ozone, NO_x, particle size and particle composition related to biomass burning impacts.

Table of Contents

List of Figures

List of Tables

List of Abbreviations

AAE	Absorption Ångström exponent
A_{meas}	Measured filter spot area
AQRP	Air Quality Research Program
A_{true}	True filter spot area
b_{abs}	Aerosol Absorption coefficient
$b_{abs_{\lambda_1}}$	Absorption coefficient at 640 nm
$b_{abs_{\lambda_2}}$	Absorption coefficient at 520 nm
$b_{abs_{\lambda_3}}$	Absorption coefficient at 450 nm
b_{scat}	Aerosol Scattering coefficient
$b_{scat_{\lambda_1}}$	Scattering coefficient at 700 nm
$b_{scat_{\lambda_2}}$	Scattering coefficient at 550 nm
$b_{scat_{\lambda_3}}$	Scattering coefficient at 450 nm
BC	Black Carbon
BrC	Brown Carbon
b_{scat}	Particle back-scatter measurement

b_{sp}	Light Scattering measurement
CO	Carbon monoxide
CAMS	Continuous Air Monitoring Site
CLAP	Continuous Light Absorption Photometer
EC	Elemental Carbon
HYSPLIT	Hybrid Single Particle Lagrangian Integrated Trajectory Model
MAE	Mass absorption efficiency
MODIS	Moderate Resolution Imaging Spectroradiometer
m^{-1}	Per meter
$m^2 g^{-1}$	Meters squared per gram
Mm^{-1}	Per Megameter
$\mu g/m^3$	Microgram per meter cubed
NASA	National Aeronautics and Space Administration
NOAA	National Oceanic and Atmospheric Administration
NO	Nitrogen monoxide
NO_2	Nitrogen dioxide
NO_x	Oxides of Nitrogen
O_3	Ozone
σ_{adj}^*	Adjusted aerosol absorption coefficient
σ_{ap}	Aerosol absorption coefficient
σ_{neph}	Uncorrected total scattering
σ_{sp}	Aerosol scattering coefficient
σ_{true}	Corrected total scattering
PPBV	Parts per billion by volume
PM	Particulate matter
$PM_{2.5}$	Particulate matter with an aerodynamic diameter of 2.5 microns or less
PMT	Photomultiplier tube
PSAP	Particle Soot Absorption Photometer

Q_{meas}	Measured flow rate
Q_{true}	True flow rate
R^2	Coefficient of Determination
SAE	Scattering Ångström exponent
SSA	Single Scattering Albedo
SOA	Secondary organic aerosol
TAP	Tricolor Absorption Photometer
TCEQ	Texas Commission on Environmental Quality
UTEP	University of Texas at El Paso
UV	Ultraviolet
VOC	Volatile Organic Compound
WRT	With respect to

1.0 Introduction

Biomass burning, which can include wildfires, agricultural burning and residential wood smoke, emits particulate matter (PM) and a wide range of gas-phase pollutants. PM emissions from biomass burning are predominantly carbonaceous, with aerosol absorbance from both black carbon (BC, or elemental carbon) and brown carbon (BrC, or light-absorbing organic carbon) (Laing et al. 2016). Biomass burning plumes can also impact ozone (O_3) and secondary organic aerosol (SOA) formation through the emission of NO_x (nitric oxide; NO and nitrogen dioxide; NO_2), sulfur dioxide, ammonia, and volatile organic compounds (VOCs). AQRP Project 16-008 and AQRP Project 16-024 identified biomass burning plumes from out-of-state as a significant source of regional background air pollution in Texas potentially impacting both O_3 and $PM_{2.5}$.

El Paso, TX is also impacted by regional biomass burning: meteorological conditions can drive biomass burning plumes into the city from across state and international boundaries (Chalbot et al. 2013). The complexity of El Paso regional air pollution is heightened by its arid climate (i.e. dust), topography, frequent temperature inversions and proximity to Ciudad Juarez, Mexico; all of which may contribute to O_3, carbon monoxide (CO), and PM (Currie et al. 2009) concentrations. The Texas AQRP Priority Research Areas for 2018-2019 identified El Paso as an area which needs additional O_3 and PM studies, including deployment of new monitoring technologies to identify episodes of biomass burning using continuous BC and BrC measurements.

Since the optical properties of BC and BrC will be utilized for source identification of biomass burning, a brief overview is warranted. Andreae and Gelencsér wrote a classic review of light-absorbing aerosols focused on BC and BrC (Andreae and Gelencser 2006). BC is defined both by its light absorption and by its refractory nature. It is formed during combustion as nearly pure elemental carbon that has a graphitic-like structure and absorbs across the visible spectrum with a mass absorption efficiency of $7.5 \pm 1.2 m^2\ g^{-1}$ (Andreae and Gelencser 2006, Bond and Bergstrom 2006). Brown carbon, BrC or light-absorbing organic carbon (Andreae and Gelencser 2006), has been identified in emissions from smoldering biomass burning fires and unlike BC, it's absorption has a strong wavelength dependence (peaking in the UV). BrC

has a very low absorbance in the visible and longer wavelengths, which are typically utilized by filter-based absorption techniques to determine BC (e.g., 600-900 nm). This difference in wavelength dependence for BrC vs BC, combined with the emission source differences, has resulted in utilization of BrC to BC absorption ratios to identify biomass burning plumes (Briggs and Long 2016, Brown et al. 2016, Garg et al. 2016, Laing et al. 2016, Becerril-Valle et al. 2017, Healy et al. 2017, Tasoglou et al. 2017, Titos et al. 2017).

Laboratory and chamber studies have identified compounds and secondary organic aerosol products which could potentially act as BrC (Lin et al. 2014, Xie et al. 2017). The precursor sources that have produced BrC in chambers when reacted in the presence of NO_x include aromatic compounds like benzene, naphthalene, and m-cresol and also the biogenic compound, isoprene. These precursor compounds produced BrC under the specific conditions in the chamber. To assess whether these types of precursors and reactions are relevant in urban areas, field or ambient measurements are needed. There have been a few field studies which have apportioned the BrC as well as measuring its impact (Washenfelder et al. 2015, Cappa et al. 2019). Both of the referenced studies apportioned the BrC with co-located aerosol mass spectrometer measurements. The studies in the southeast US (Washenfelder et al. 2015) and in Fresno, CA (Cappa et al. 2019) both report that biomass burning dominates BrC. The study in Fresno had a contribution from an aged, nitro-organic factor as well (Cappa et al. 2019), however, the biomass burning factor had a stronger contribution and a distinct temporal trend that matched the BrC absorption. In summary, although it is possible to have other BrC contributions, additional measurements, temporal trends, statistical methods and supporting remote sensing can facilitate clean separation of biomass burning BrC.

Considerable work has been done to quantify and characterize BC and aerosol absorption in the atmosphere using a variety of instrumentation and protocols (Snyder and Schauer 2007, Sandradewi et al. 2008b, Ram and Sarin 2009, Ram et al. 2010, Subramanian et al. 2010, Kondo et al. 2011, Müller et al. 2011, Bahadur et al. 2012, Schwarz et al. 2012, Dallmann et al. 2014, Zhi et al. 2014, Laing et al. 2016, Ogren et al. 2017, Sinha et al. 2017). The most effective campaigns for investigation of BC and BrC have included more than one absorption instrument. This guarantees that the results can be compared across a variety of previous studies, but still incorporate the advancements of new technologies. Therefore, $(BC)^2$

El Paso includes both TAP and aethalometer measurement of wavelength-dependent aerosol absorption.

Cost-effective options for real-time monitoring have included many filter-based techniques, where light transmission through a filter media is measured at short intervals while atmospheric PM is slowly accumulating. There are uncertainties associated with this type of measurement, which can be large. Uncertainties associated with the filter can include: a lack of reference standard for quantification of BC, uncertainty in the scattering correction by the filter and PM loading resulting in shadowing effects (Bond et al. 1999, Müller et al. 2011). Additional uncertainties include specificity of light source wavelength, flow rate, and definition of size of sample area (Müller et al. 2011). To assess the "best" instrument for a given application, these uncertainties need to be adequately addressed.

To address on-going issues with other filter-based, realtime BC and BrC instruments (i.e. high frequency of manual filter changes, problematic and contentious correction schemes for aerosol scattering and other filter effects), NOAA developed and constructed an aerosol absorption instrument, the continuous light absorption photometer or CLAP (tricolor absorption photometers, TAP, Bechtel, Inc. is the commercial version) that fulfilled the needs of long-term monitoring, improved corrections, multiple wavelengths, high sensitivity and low noise, precisely defined filter spot areas, temperature stabilization, with same correction factors as the PSAP, very low cost and very small instrument footprint (Ogren et al. 2017). To minimize uncertainty in absorption measurements, and to improve aerosol classification through complementary measurement of aerosol scattering, the $(BC)^2$ El Paso campaign deployed a three-wavelength nephelometer (Laing et al. 2016, Ogren et al. 2017). The TAP represents the cutting edge of filter-based photometers and was purchased, deployed, and validated for long-term application during $(BC)^2$ El Paso in 2018-19.

Influence of biomass burning plumes was identified utilizing the absorption measurements of BC and BrC, using methodology based on recently published studies (Laing et al. 2016, Wang et al. 2016, Becerril-Valle et al. 2017, Healy et al. 2017, Titos et al. 2017). Specifically, high AAE values indicated the presence of BrC (1.5-4.5) and influence of biomass burning, while the typical urban combustion sources dominated by BC had a lower AAE value, which remained near 1. Higher concentrations of BrC in the aerosol results in a higher AAE

value due to it's ability to selectively absorb short wavelengths. Motor vehicle exhaust, or similar fossil fuel combustion has been demonstrated to have an AAE value dominated by BC while biomass burning has been demonstrated to contribute the higher, BrC-influenced AAE (Sandradewi et al. 2008a). AAE values can be calculated for specific absorption coefficient pairs or through the calculation of the slope of the difference in absorption coefficients over multiple wavelengths. Most recently, Laing et al. and Schmeisser et al., outlines the use of TAP aerosol light absorption coefficient measurements (σ_{abs}), nephelometer aerosol light scattering coefficient measurements (σ_{scat}) and CO to further characterize the influence of transported biomass burning plumes (Laing et al. 2016, Schmeisser et al. 2017). Laing et al. identified that long-range transport events had lower AAE values and higher σ_{abs} to CO enhancement ratios ($\Delta\sigma_{abs}/\Delta CO$) as compared to more regional transport. This difference in AAE values was attributed to two different possibilities. However, this example is for a remote site, and the use of enhancement ratios needs to be tested for Texas urban areas.

The AAEs reported in other studies may be site specific as transport time, combustion conditions and local mixing of sources may have an impact on the resultant optical properties. This is the rationale for the long field campaign that extends beyond the biomass burning season in El Paso: so that a site specific AAE average without biomass burning can be determined. Additional validation/instrumentation will be used during this project to confirm wildfire impacts (i.e., CO, and $PM_{2.5}$ from TCEQ monitoring sites in El Paso). Once validation is completed for a specific site, the absorption instruments may be sufficient in themselves to identify and quantify biomass burning contribution. This will be investigated during the $(BC)^2$ El Paso project, where a nephelometer will be deployed with the TAPs and aethalometer while synoptic TCEQ monitoring network data will be utilized for confirmation and further characterization.

While previous studies have focused on identification of biomass burning influence at remote sites, the $(BC)^2$ El Paso study was an urban study. This confounded the ability to identify by concentration differences or enhancement ratios. However, since the AAE is assessing the wavelength dependence of absorption, an intrinsic property, it has the unique utility to identify biomass-burning influence under lower concentration conditions.

2.0 Project Design

A long-term field campaign, the Black Carbon, Brown Carbon El Paso or $(BC)^2$ El Paso campaign, deployed a suite of small footprint, low power, low maintenance, optical instruments in El Paso, TX (March to June 2019). This suite includes two, three-wavelength TAPs, a three-wavelength nephelometer, and a seven-channel aethalometer. All optical measurements were conducted on particulate matter with an aerodynamic diameter of 2.5 microns or less ($PM_{2.5}$). Aerosol ($PM_{2.5}$) absorption coefficients (Mm^{-1}) for ultraviolet (365 nm), green (520 nm), and red (640 nm) wavelengths were collected using both TAP instruments deployed using a one-hour alternating measurements. The dual goals of this deployment were to address scientific air quality questions of frequency, seasonality, and optical properties of biomass burning plumes in El Paso as well as the instrument evaluation of the TAP for application in long-term monitoring at urban sites in Texas. The science questions utilize aerosol absorption measurements at three different wavelengths (e.g., UV, green, and red wavelengths) for March through June 2019 to 1) identify biomass burning plumes and 2) use the range in observed absorption Ångström exponents (AAE) to characterize the biomass burning plumes. The results of this study could be used to develop effective strategies to improve air quality in El Paso. In addition, the instrument evaluation of the TAP will help TCEQ determine the suitability of this instrument for future deployment in Texas for characterization of biomass burning impacts.

Instrumentation was installed in the Baylor Air Quality Trailer, which was located adjacent to the TCEQ CAMS 12 (UTEP) air monitoring site. This trailer has previously been used for both trace gas and aerosol sampling and has provisions for the installation of sampling equipment and inlets. Instrument integration and trailer preparation occurred in Waco at Baylor University prior to deployment for $(BC)^2$ El Paso. A logbook was kept for instrument operators to log information on the instruments and maintenance.

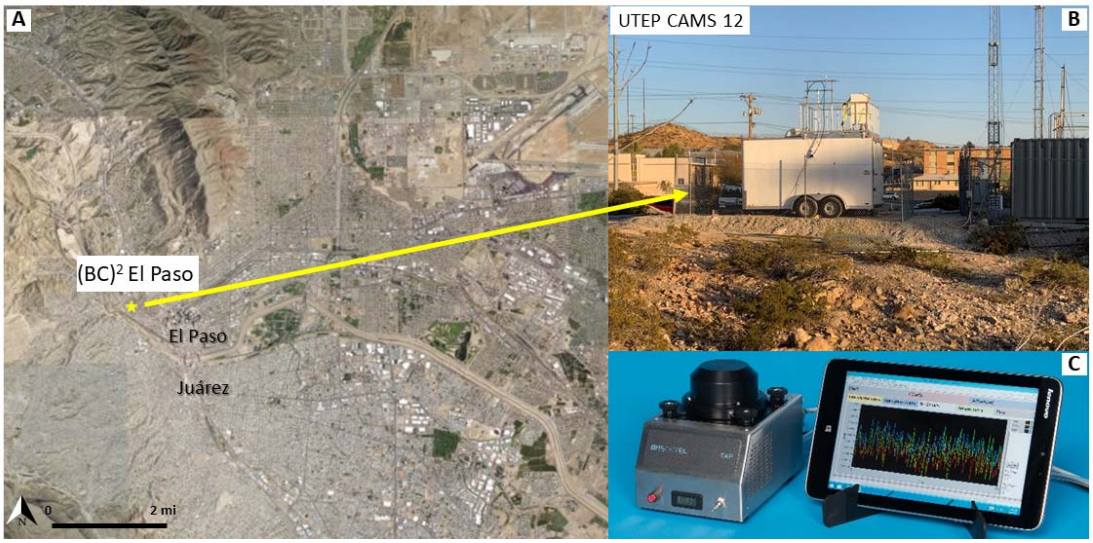

Figure 1. (A) Site location for $(BC)^2$ El Paso campaign. (B) Baylor Air Monitoring Trailer co-located with the CAMS 12 (UTEP) site. (C) A TAP instrument with computer interface.

3.0 Methods

3.1.1 Optical Absorption Measurements – Tricolor Absorption Photometer

A 3λ tricolor absorption photometer (TAP; Model 2901, Brechtel Inc., Hayward, CA) measures aerosol light absorption at wavelengths 365 (UV), 520 (green), and 640 (red) nm. The TAP uses 10 solenoid valves to cycle through 8 filter spots and 2 reference filter spots. The LED light source simultaneously shines through the sample and reference spots loaded with 47 mm glass-fiber filter (Brechtel TAP-FIL100). The reference spot allows a differential measurement approach in the TAP so the increase in light attenuation due to deposited particles on the sample spot can be largely separated from filter effects. The TAP is set to rotate to the next filter spot when a filter spot's transmission reaches 50% attenuation and the reference channel gets altered whenever the sample spot is changed. Each of the 8 sample spots is separated from the other by O-rings that clamp the filter material to prevent any inter-spot leakage. The air flow passes through the filter and into a solenoid valve controlled by the TAP Reader software.

Manual filter changes are the primary TAP maintenance. These filter changes on the TAP require minimal tools and consumables and little time. Items required for a filter change include a torque driver, replacement filter, tweezers, and zip-lock plastic bag. The standard

operating procedure for changing a TAP filter has been described (with photos) in the TAP Model 2901 UV system manual.

3.1.2 Optical Scattering Measurements – Nephelometer

Light scattering (b_{sp}) was measured using a TSI Model 3563 nephelometer. In most integrating nephelometers, a white light source is used to illuminate the air sample, and light scattered by particles (and gases) at a particular wavelength is measured using a photomultiplier tube. In this project, a three-wavelength instrument is used (450, 550, and 750 nm; blue, green, and red, respectively). Filters in front of the PMT's (Photomultiplier tubes) are used for wavelength selection. In addition, the TSI instrument provides a separate measurement of particle back-scatter (b_{scat}). The instrument automatically calculates Rayleigh scattering from internally measured temperature and pressure and corrects the reported signal for those factors. Averaging time was determined based on the performance of the aethalometer and TAP instruments and set to a five minute average.

3.1.3 Optical Absorption Measurements – Aethalometer

The AE42 aethalometer (Magee Scientific, Berkeley, CA) measures light attenuation at seven different wavelengths (370, 470, 520, 590, 660, 880 and 950 nm). The AE42 used in the study had been purchased in 2010. The aerosol stream is drawn through a spot on a filter tape at user-set flow rate (typically ~ 5 l min^{-1}). The detector measures the intensities of light transmitted through the sample spot versus the unexposed portion of the tape (reference spot) as sampled aerosol is being continuously deposited on the quartz fiber filter tape. As the absorbing aerosols accumulate on the sample spot, the intensity of light transmission through the sample spot decreases. The aethalometer manufacturer (Magee Scientific) calibrated the instrument based on the assumption that the change in aerosol light attenuation coefficient (m^{-1}) is proportional to BC concentration (g m^{-3}) through a constant called specific absorption cross section (m^2 g^{-1}) and the default output is BC at each wavelength. The aerosol absorption coefficient is derived for each wavelength using reported corrections and back calculations from the literature.

3.1.4 Filter Area and Wavelength Corrections

Bond et al. presented correction of particle soot absorption photometer to account the error in filter-based measurement of light-absorbing aerosols (Bond et al. 1999). As the TAP operates under the same principles, this correction will be applied to the TAP in the current project (Ogren et al. 2017). This correction uses a reference absorption determined as the difference between light extinction and light scattering by suspended particles. Bond et al. suggested that differences within instruments requires correction for true flow rates (Q_{true}) and filter spot area (A_{true}) and hence the adjusted absorption coefficient (σ_{adj}^{*}) for PSAP was derived as below:

$$\sigma_{adj}^{*} = (Q_{PSAP} / Q_{true}) (A_{true} / A_{ref}) \sigma_{PSAP} \quad (1)$$

where Q_{PSAP}, A_{true} and σ_{PSAP} are flow rate, filter spot area and reported absorption coefficient of PSAP.

Ogren (2010) further elaborated the correction and the alternative σ_{adj} was derived (Ogren 2010). The filter spot area internally used by PSAP (A_{PSAP} = 17.83 mm^2) and the measured spot area of the manufacturer reference instrument (A_{ref} = 20.43 mm^2) was corrected as below:

$$\sigma_{adj} = (A_{PSAP} / A_{ref}) \sigma_{adj}^{*} = (17.83 / 20.43) \sigma_{adj}^{*} = 0.873 \sigma_{adj}^{*} \quad (2)$$

Equations (1) and (2) are based on equations (1 and 12) in Bond et al and equation (6) in Ogren (2010) which further yields the true aerosol absorption coefficient, calculated as:

$$\sigma_{ap} = 0.873 (Q_{PSAP} / Q_{true}) (A_{true} / A_{PSAP}) (\sigma_{PSAP} / K_2) - (K_1 / K_2) \sigma_{sp} \quad (3)$$

where σ_{ap} and σ_{sp} are aerosol absorption coefficient and aerosol scattering coefficients respectively and K_1 and K_2 are the calibration constants representing the response of the instrument to scattering and absorption respectively. Bond et al also reported the numerical values of K_1 and K_2 to be 0.02 ± 0.02 and 1.22 ± 0.20, respectively when the measurements were made at a wavelength of 550 nm (Bond et al. 1999).

Later Virkkula et al. (2005) reported that the correct wavelength of the instrument to be 574 nm instead of 550 nm used by Bond et al. (Virkkula et al. 2005). After the wavelength adjustment Ogren reported the correction for measurements of scattering and absorption at wavelength λ becomes

$$\sigma_{ap}[\lambda] = 0.85\ (Q_{PSAP} / Q_{meas})\ (A_{meas} / A_{PSAP})\ (\sigma_{PSAP}[\lambda] / K_2) - (K_1 / K_2)\ \sigma_{sp}[\lambda] \quad (4)$$

where Q_{meas} and A_{meas} are the measured flow rate and filter spot areas of the instrument. In TAP, $Q_{meas} = Q_{PSAP}$ and $A_{meas} = A_{PSAP}$, so equation (4) simplifies to

$$\sigma_{ap}[\lambda] = 0.85\ (\sigma_{PSAP}[\lambda] / K_2) - (K_1 / K_2)\ \sigma_{sp}[\lambda] \quad (5)$$

Measurement of real-time σ_{sp} data requires that a nephelometer run in parallel to the TAP. As notified in the TAP user manual (Photometer, n.d.), depending on the version of software, we have an option to define σ_{sp}. If we don't have this option, then the program calculates

$$\sigma_{ap}[\lambda] = 0.85\ (\sigma_{PSAP}[\lambda] / K_2) \quad (6)$$

Angular truncation correction of total scattering coefficient

The nephelometer sensitivity is biased due to two factors- angular truncation and nonlambertian error (Anderson and Ogren, 2007). Truncation error is caused due to the nonidealities in near-forward light scattering from 0 to 7 degrees, i.e. the scattering measurements are not performed within this truncation angles due to geometric blockage in the instrument (Moosmuller and Arnott, 2003). Forward truncation error is higher in the absorbing aerosols by nearly two folds than the non-absorbing aerosols, thus the truncation correction is important in the absorbing aerosol dominated locations. Although the truncation error is below 10% for fine particles, the error can be as large as 20-50% for particles above 1μm diameter (Moosmuller and Arnott, 2003). Since both truncation correction and Ångström exponent are dependent upon particle size, Anderson and Ogren (2007) derived the correction using Mei theory which can expressed as:

$$C_{ts} = a + b\ \alpha^*_{ts} \quad (7)$$

where the values for coefficients a and b are listed in the literature by Anderson and Ogren (2007); α^*_{ts} is the scattering Ångström exponent using uncorrected data at 450, 550 and 700 nm. The α^*_{ts} at 450nm is calculated as α (450/550), at 550nm as α (450/700) and at 700nm as α (550/700).

Therefore, the corrected total scattering coefficient can be calculated as:

$$\sigma_{true} = C_{ts} \cdot \sigma_{neph} \quad (8)$$

where, σ_{true} is corrected total scattering and σ_{neph} is uncorrected total scattering measured by nephelometer prior truncation error correction.

The uncertainty associated with Anderson and Ogren (2007) angular truncation correction technique was evaluated by Bond et al. (2009) and confirmed that the associated uncertainties is small.

3.1.5 Ångström Exponents Calculations

The nephelometer and TAP measurements are used to calculate the Ångström exponents for characterization of the wavelength dependency of aerosol absorption and scattering. The Ångström exponent is calculated as the negative slope of the linear fit of the optical parameter versus the wavelengths on a log-log plot (Moosmüller and Chakrabarty, 2011). The Ångström exponents for three wavelength bands can be represented using the following equation (Bergstrom et al., 2007; Kirchstetter et al., 2004; Schnaiter, 2005; Schnaiter et al., 2006).

$$\text{Absorption Ångström Exponent} = - \frac{\ln (babs_{\lambda 1,}\, babs_{\lambda 2,}\, babs_{\lambda 3,})}{\ln(\lambda 1, \lambda 2, \lambda 3)} \quad (9)$$

The absorption Ångström exponent (AAE) is calculated with the absorption coefficient data measured using the TAPs at 640, 520, 365 nm ($\lambda 1,\ \lambda 2,$ and $\lambda 3$ respectively).

In this study, the SAE is calculated with the scattering coefficient measured using the nephelometer (TSI 3563) at 700, 550, 450 nm ($\lambda 1,\ \lambda 2,$ and $\lambda 3$ respectively). SAE is an intrinsic property of the aerosol derived based on the wavelength dependency of the aerosol scattering. SAE is inversely related to the particle size which indicates that larger particles will have smaller SAE and vice-versa (Schmeisser et al., 2017). The Angstrom exponents for three wavelength bands can be represented using following equation (Bergstrom et al., 2007; Kirchstetter et al., 2004; Schnaiter, 2005; Schnaiter et al., 2006).

$$\text{Scattering Angstrom Exponent} = - \frac{\ln (bscat_{\lambda 1,}\, bscat_{\lambda 2,}\, bscat_{\lambda 3,})}{\ln(\lambda 1, \lambda 2, \lambda 3)} \quad (10)$$

3.1.6 Single Scattering Albedo

The single scattering albedo (SSA) is the ratio of scattering to the total extinction. SSA is considered as the proxy to estimate the radiative effects of the atmospheric aerosols and is calculated using the following equation:

$$SSA = \frac{b_{scat}}{b_{scat} + b_{abs}} \quad (11)$$

where; b_{scat} and b_{abs} are the scattering coefficient and absorption coefficients, respectively. In conjunction with the AAE and SAE, the SSA can be used for aerosol source characterization.

3.1.7 MODIS satellite data

Near real-time satellite data from NASA's Moderate Resolution Imaging Spectroradiometer (MODIS) instrument aboard the Aqua and Terra satellites (Product Title: MODIS/Aqua+Terra Thermal Anomalies/Fire locations 1km FIRMS V006 NRT) was utilized to determine the locations of active fires across North America. The data was downloaded daily and imported to Google Earth Pro (version 7.3.2.5776 (32-bit)) to allow for simultaneous evaluation with the HYSPLIT Back Trajectories for possible biomass burning influences. The fire data can be downloaded at https://earthdata.nasa.gov/active-fire-data

3.1.8 HYSPLIT Back Trajectories

Developed by NOAA's Air Resources Laboratory, the Hybrid Single-Particle Lagrangian Integrated Trajectory model (HYSPLIT) was utilized to determine the origin of the air masses influencing the $(BC)^2$ El Paso site (Stein et al. 2015, Rolph et al. 2017). Backward trajectories were run at 500 meters above ground level, had a 72-hour duration, and new trajectories were started every 6 hours. The trajectories were downloaded and imported to Google Earth Pro (version 7.3.2.5776 (32-bit)) for evaluation with the MODIS satellite data to determine possible biomass burning influences. Back trajectories can be computed at https://ready.arl.noaa.gov/HYSPLIT_traj.php

3.1.9 MATLAB

Real-time TAP, nephelometer, and trace-gas data from the $(BC)^2$ El Paso site was imported to MATLAB (version R2018a) for qualitative and quantitative data analysis. Using a code writen specifically for this analysis, AAE, SAE, SSA, and absorption and scattering coefficients plots were created daily as part of a check on instrument operations and to determine if a site visit was needed.

3.1.10 Particulate Matter Sampling

Filter-based fine particulate matter ($PM_{2.5}$) sampling was conducted on a periodic basis to archive urban baseline and fire events on filters for future analysis. The mass absorption efficiency (MAE) of BC is used by the aethalometer to calculate BC from light attenuation. Filter-based analysis of organic and elemental carbon (EC, as a proxy for BC) can be used to check the El Paso MAE under baseline conditions and fire events. This was not finalized under the current campaign, but filters have been collected and archived for future analysis as needed.

4.0 Results

4.1 Tricolor Absorption Photometers Time Series Data

4.1.1 Aerosol Absorption Five Minute Averages - Tricolor Absorption Photometers

Figures 2 through 4 report five-minute averages of the aerosol ($PM_{2.5}$) absorption coefficients (Mm^{-1}) for ultraviolet (365 nm), green (520 nm), and red (640 nm) wavelengths using combined datasets from the two TAP instruments. TAPs were deployed (March to June) using alternating one-hour measurements in conjunction with a nephelometer, aethalometer, and trace gas instrumentation. Absorption coefficient data integrates smoothly across the two instruments and shows variability of short time intervals.

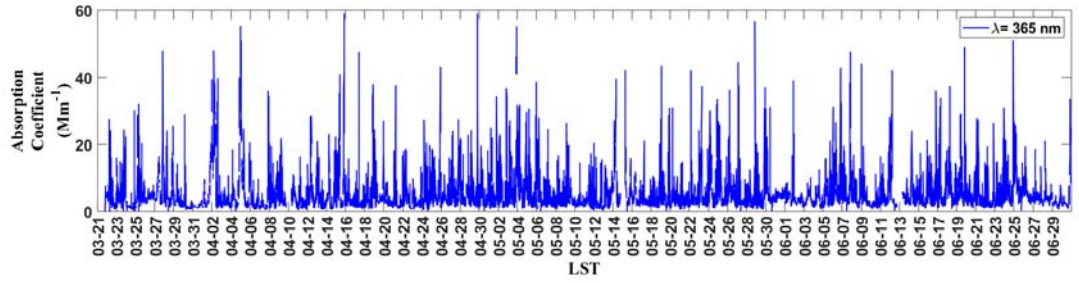

Figure 2. The aerosol absorption coefficient (Mm^{-1}) measured at 365 nm (ultraviolet) and reported as 5 min averages.

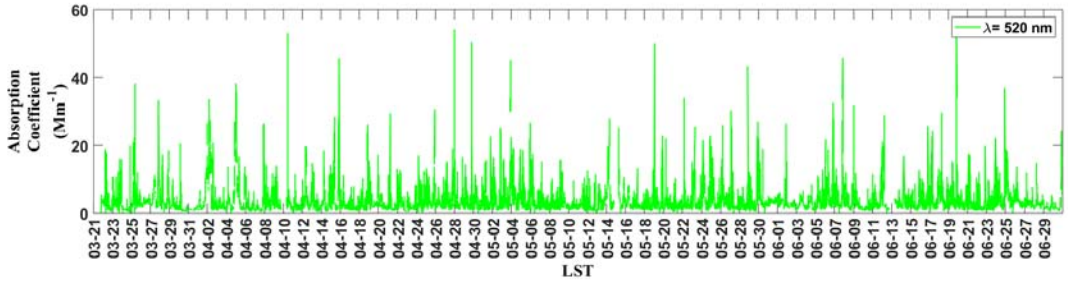

Figure 3. The aerosol absorption coefficient (Mm^{-1}) measured at 520 nm (green) and reported as 5 min averages.

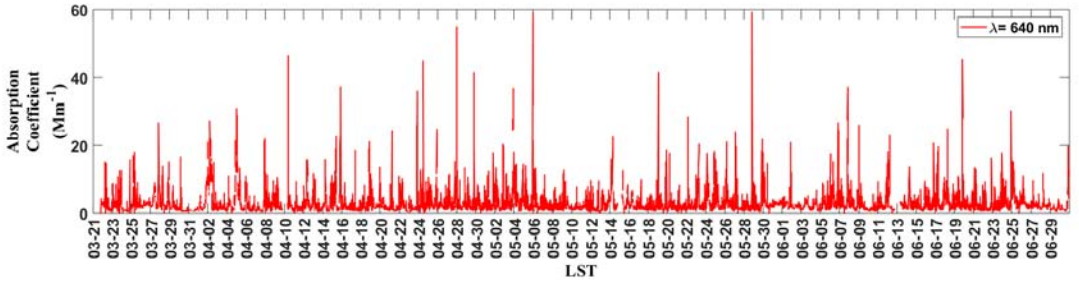

Figure 4. The aerosol absorption coefficient (Mm^{-1}) measured at 640 nm (red) and reported as 5 min averages.

Figure 5 shows the aerosol AAE calculated by ultraviolet (365 nm), green (520 nm), and red (640 nm) wavelengths measured using both TAP instruments. AAE for the entire campaign (March to June) was calculated using equation 9. Comparing with the absorption coefficient above, the AAE is a ratio and has significantly less variability over the campaign, as it does not

change with aerosol concentration but changes as the wavelength dependency of the absorption changes. This allows for easier identification of biomass burning influence in an urban atmosphere with mixed combustion sources.

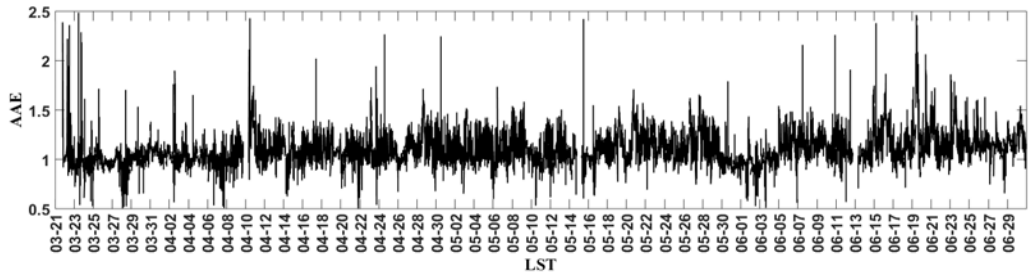

Figure 5. The aerosol absorption Ångström exponent in 5 min averages.

4.1.2 Absorption Weekly Averages - TAP

Figures 6 reports weekly averages of the aerosol ($PM_{2.5}$) absorption coefficients (Mm^{-1}) for ultraviolet (365 nm), green (520 nm), and red (640 nm) wavelengths.

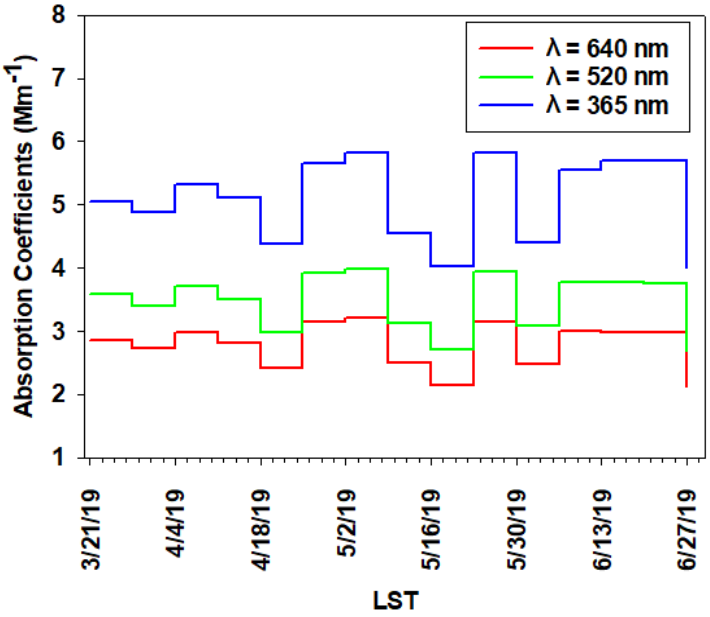

Figure 6. Weekly averages of aerosol absorption coefficients (Mm^{-1}) measured at the 365, 520, and 640 nm using the TAP instruments.

Figure 7 reports weekly averages of the AAE using ultraviolet (365 nm), green (520 nm), and red (640 nm) wavelengths. A distinct upward trend is noted in the AAE. Increasing

influence from biomass burning will push the AAE above 1.0. This trend is not evident in the absorption coefficient weekly data (Figure 6) and indicates the advantage of the AAE calculation for identifying biomass-burning plumes.

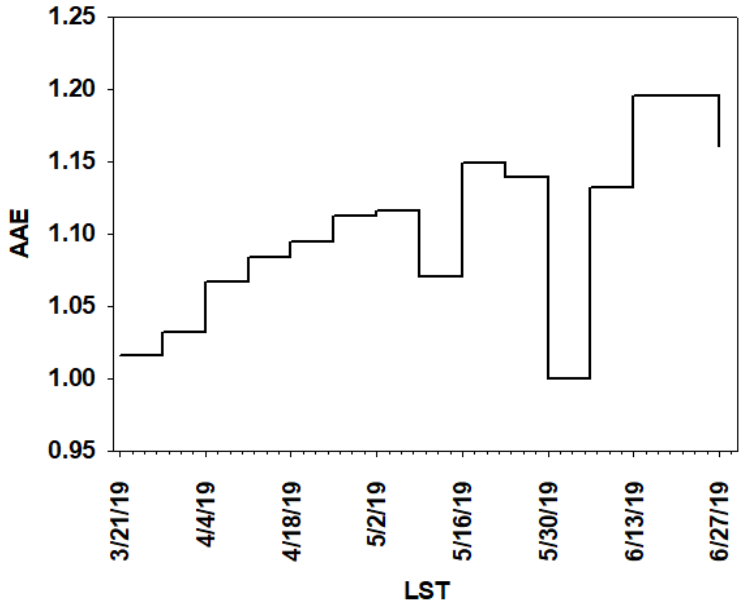

Figure 7. Weekly averages of the aersosol absorption Ångström exponent.

4.1.3 Diel Variation in Aerosol AAE – TAP

Figure 8 shows the diel variation aerosol in AAE for the entire campaign. This is plotted to determine whether there is a diel pattern in biomass burning influence at the site. No such pattern is evident.

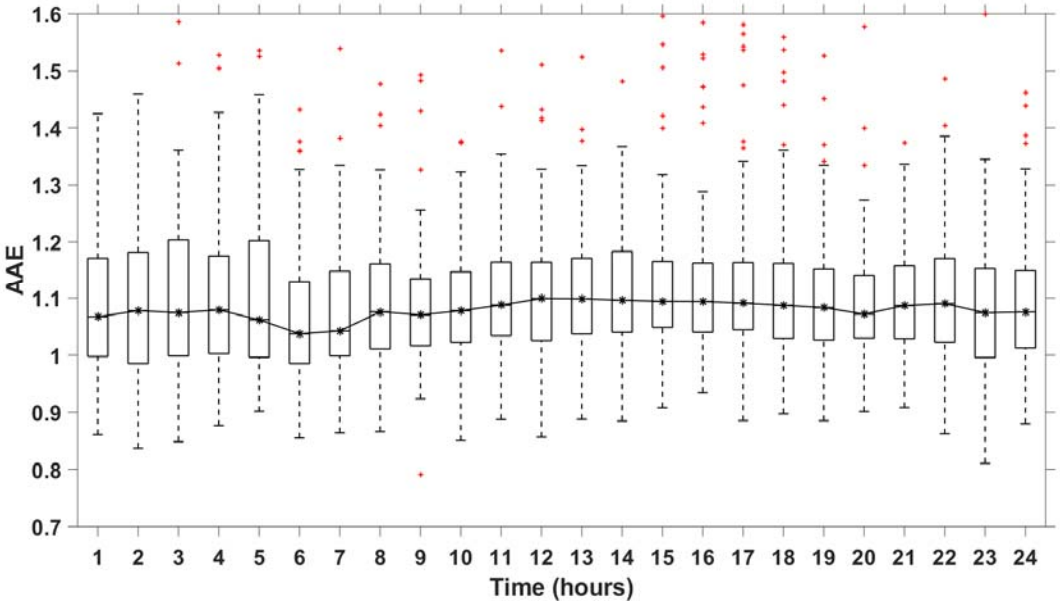

Figure 8. Diel variation in AAE.

4.2 Nephelometer Time Series Data

4.2.1 Aerosol Scattering Five Minute Averages

Figures 9 through 11 report five minute averages of the aerosol ($PM_{2.5}$) scattering coefficients (Mm^{-1}) for blue (450 nm), green (550 nm), and red (700 nm) wavelengths using the nephelometer instrument. Dust events will increase the scattering coefficient.

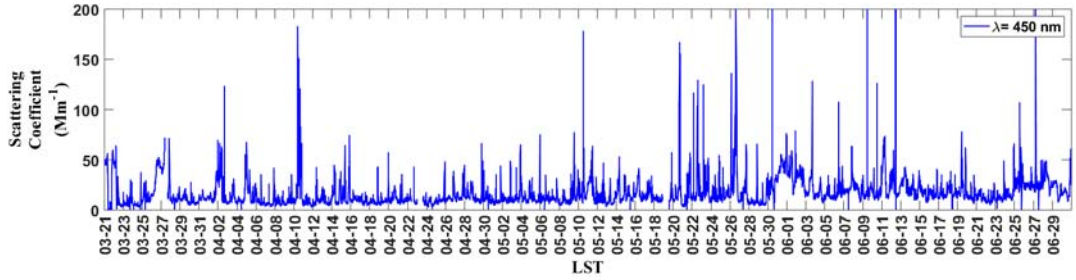

Figure 9. Aerosol scattering coefficient (Mm^{-1}) measured at the 450 nm (blue) and reported as 5 min averages.

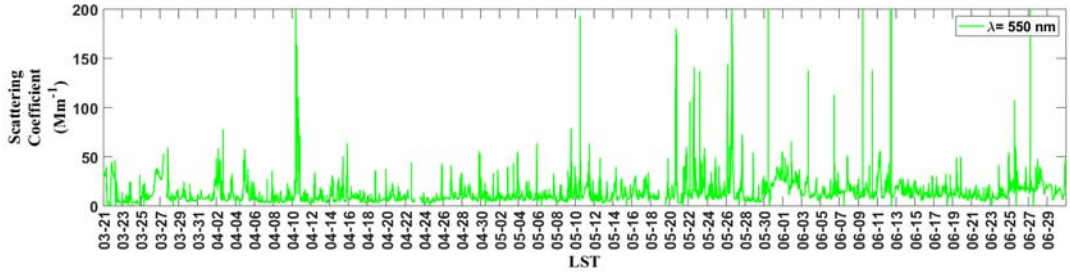

Figure 10. Aerosol scattering coefficient (Mm^{-1}) measured at the 550 nm (green) and reported as 5 min averages.

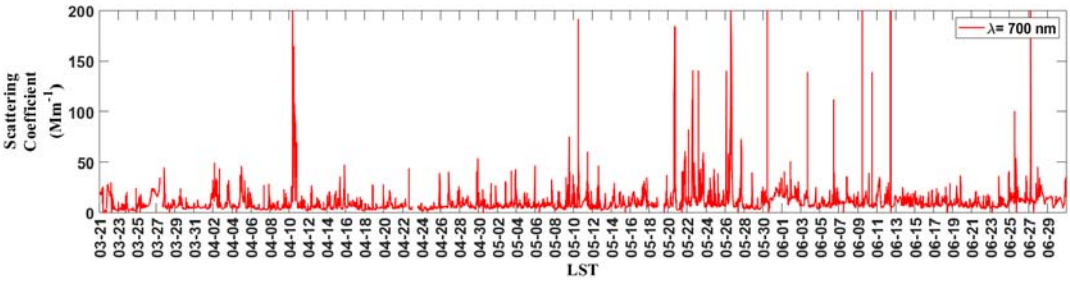

Figure 11. Aerosol scattering coefficient (Mm^{-1}) measured at the 700 nm (red) and reported as 5 min averages.

Figure 12 shows the aerosol SAE using blue (450 nm), green (550 nm), and red (700 nm) wavelengths measured using a nephelometer. SAE for the entire campaign (March to June) were calculated using equations 10 and reported using five minute averages. The SAE can be used to identify dust events with greater distinction than simply using the scattering coefficient. SAE near zero are indicative of dust events. A combination of SAE, AAE and SSA has been employed to give source characterization.

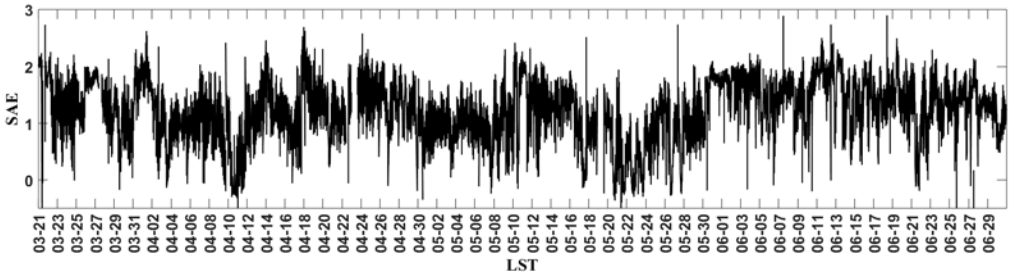

Figure 12. Aerosol scattering Ångström exponent 5 min averages.

Figures 13 through 15 report the aerosol ($PM_{2.5}$) scattering albedo for blue (450 nm), green (550 nm), and red (700 nm) wavelengths using the nephelometer instrument. SAE for the campaign (March to June) were calculated using equation 10 and reported using five minute averages.

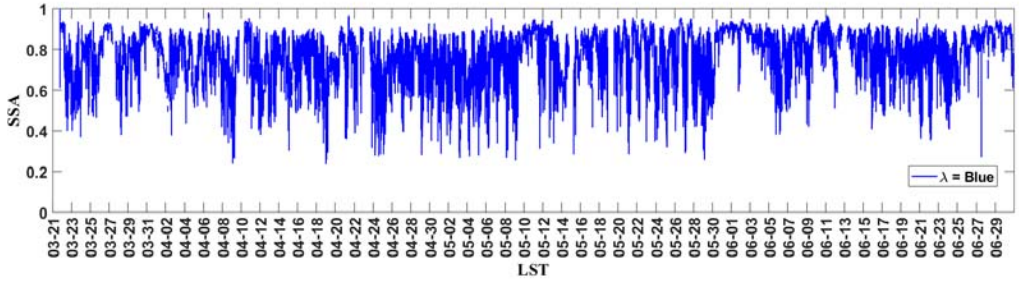

Figure 13. Nephelometer Single Scattering Albedo measured at the 450 nm (blue) and reported as 5 min averages.

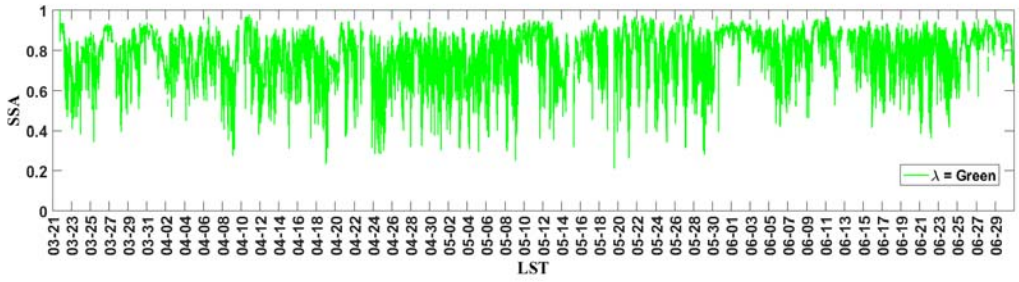

Figure 14. Nephelometer Single Scattering Albedo measured at the 550 nm (green) and reported as 5 min averages.

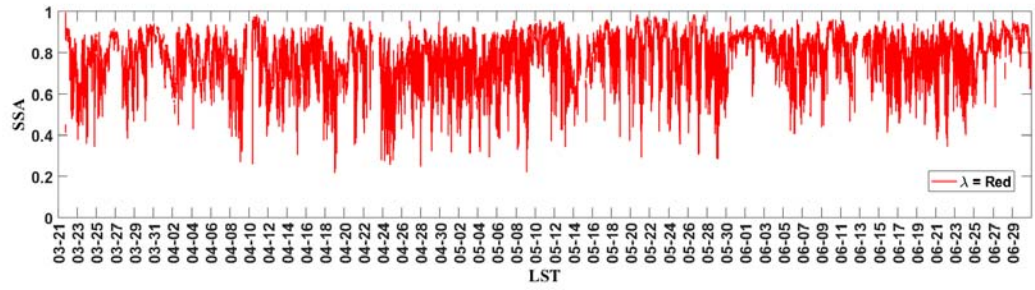

Figure 15. Nephelometer single scattering albedo measured at the 700 nm (red) and reported as 5 min averages.

4.2.2 Aerosol Scattering Weekly Averages

Figure 16 reports weekly averages of the aerosol scattering coefficients (Mm^{-1}) for blue (450 nm), green (550 nm), and red (700 nm) wavelengths measured using a nephelometer. May had the highest scattering coefficients.

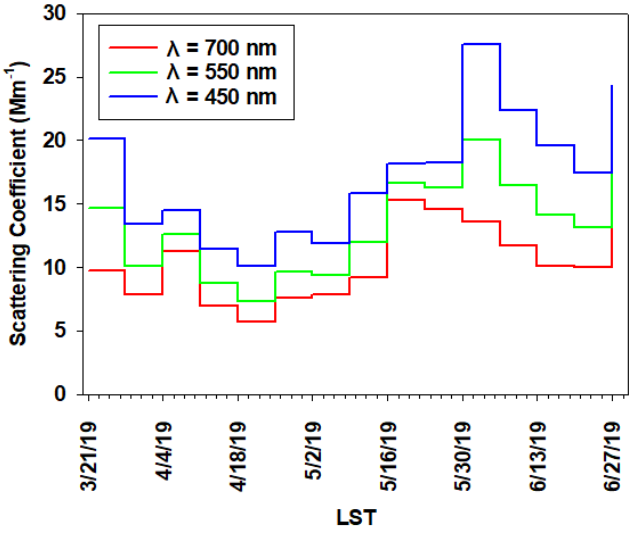

Figure 16. Weekly averages of nephelometer scattering coefficients (Mm^{-1}) measured at the 450, 550, and 700 nm.

Figure 17 reports weekly averages of the aerosol SSA using blue (450 nm), green (550 nm), and red (700 nm) wavelengths.

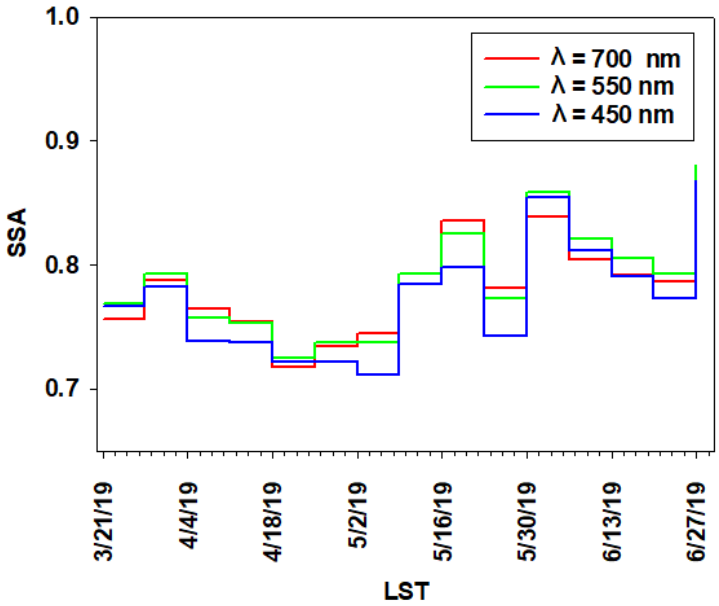

Figure 17. Weekly averages of nephelometer single scattering albedo (Mm^{-1}) measured at the 450, 550, and 700 nm.

Figure 18 reports weekly averages of the SAE. The SAE is lowest during early April and mid-May which reflects the peak in scattering coefficients in Figure 17. This indicates dust events.

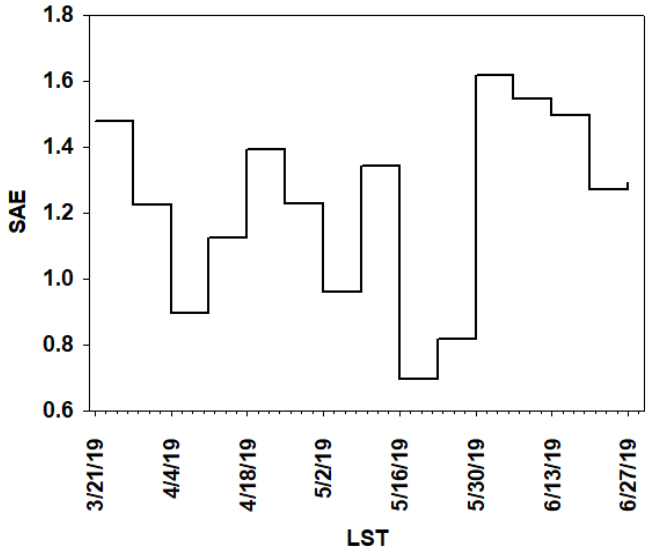

Figure 18. Weekly averages of the aerosol scattering Ångström exponent.

4.2.3 Diel Variation in Aerosol SSA and SAE

The diel variation aerosol SSA for 450 nm (Figure 19), 550 nm (Figure 20), and 700 nm (Figure 21) measured using the nephelometer. SSA for the entire campaign (March to June) were calculated using equations 11 and five minute averages. High SSA (i.e. SSA > 0.9) indicates that the atmosphere is dominated by scattering aerosols while low SSA (i.e. SSA < 0.9) indicates that the atmosphere is dominated by absorbing aerosols. The diel variation in SSA demonstrates influence from BC associated with morning rush hour traffic while the midday has more influence from scattering aerosol.

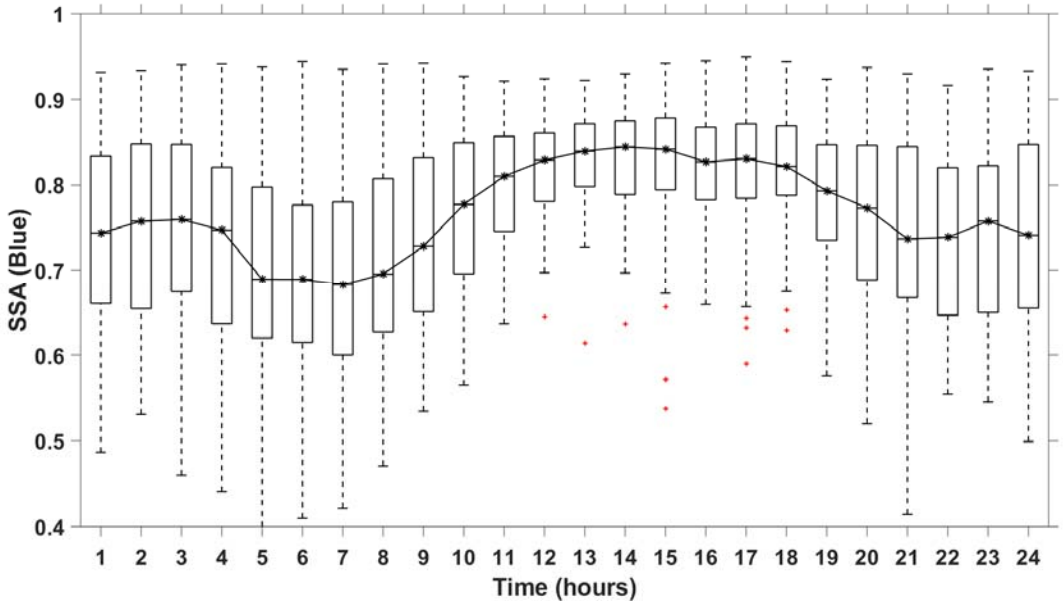

Figure 19. Diel variation in SSA using a 450 nm (blue).

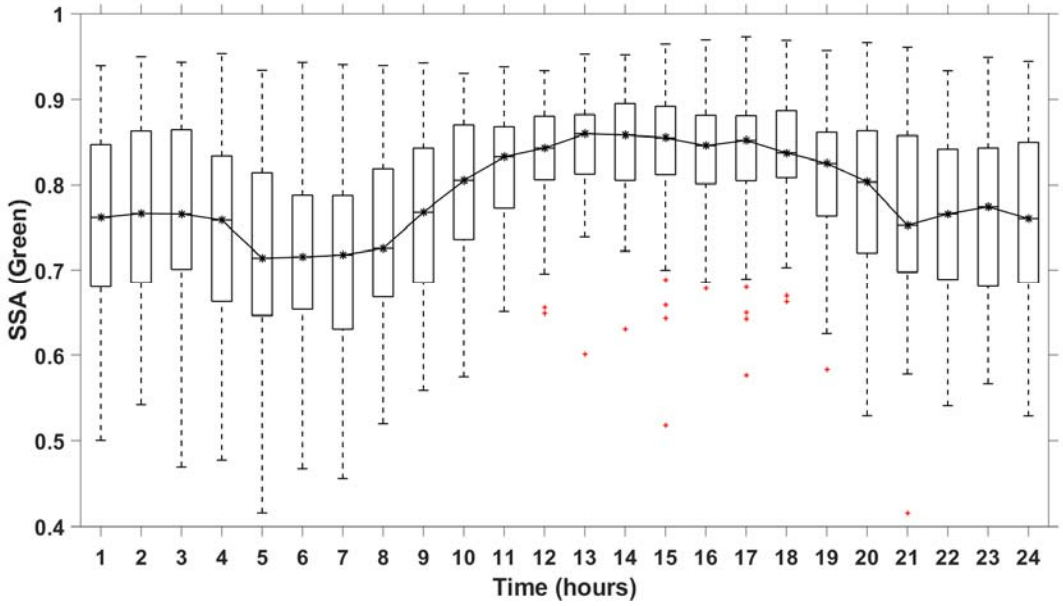

Figure 20. Diel variation in SSA using a 550 nm (green).

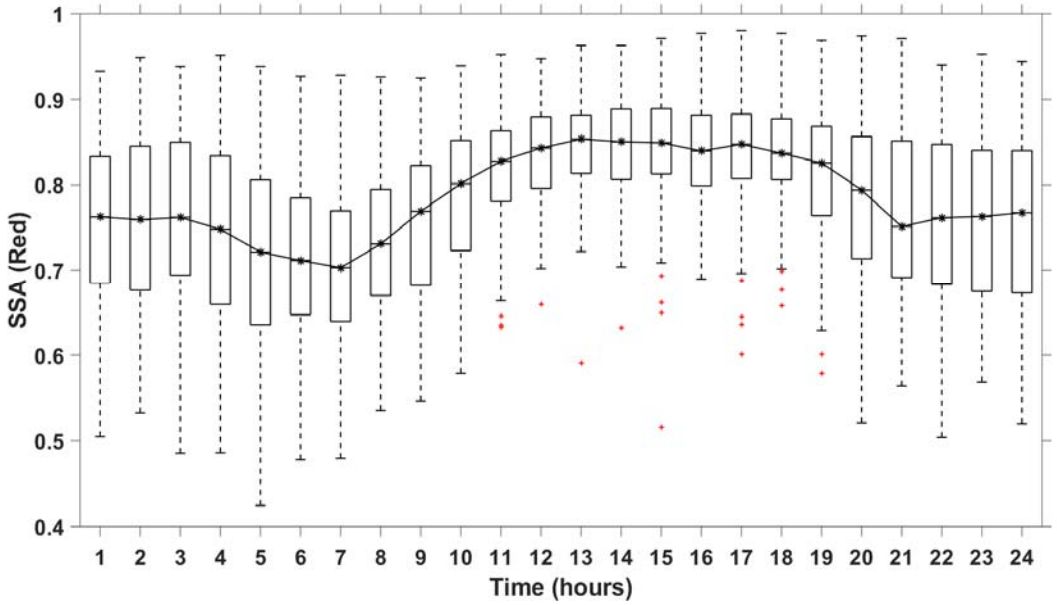

Figure 21. Diel variation in SSA using a 700 nm (red).

Figure 22, shows the diel variation aerosol SAE from the nephelometer. SAE for the entire campaign (March to June) were calculated using equations 9 and five minute averages.

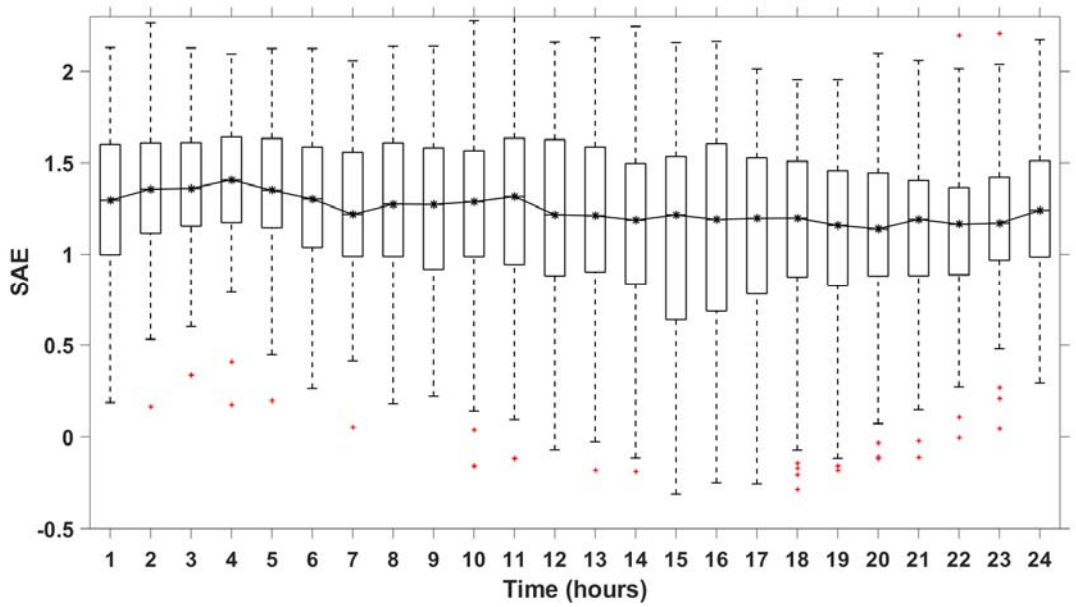

Figure 22. Diel variation in SAE based off of 5 minute averages.

4.3 Aethalometer Time Series Data

4.3.1 Aerosol Absorption Five Minute Averages - Aethalometer

Figures 23 through 29, shows aerosol ($PM_{2.5}$) black carbon (BC) concentrations ($\mu g/m^3$) measured at 370, 470, 520, 590, 660, 880, and 950 nm using an aethalometer. BC concentrations for the entire campaign (March to June) were reported using five minute averages. The aethalometer was deployed (March to June) in conjunction with a two TAPs, nephelometer, and trace gas instrumentation. Instrumentation were housed in the Baylor Air Quality Trailer which was adjacent to the TCEQ CAMS 12 UTEP site.

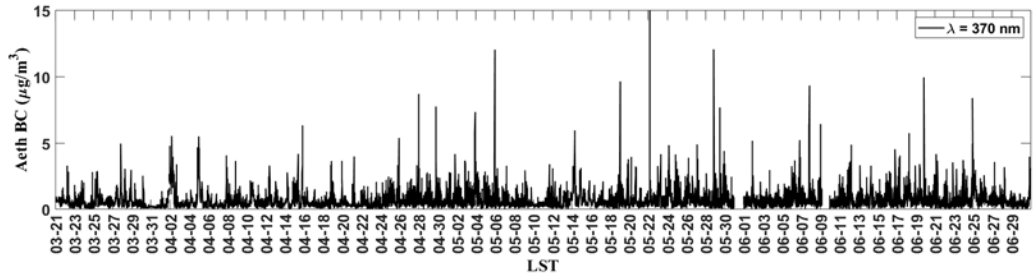

Figure 23. Aerosol black carbon concentrations ($\mu g/m^3$) measured at the 370 nm and reported as 5 min averages.

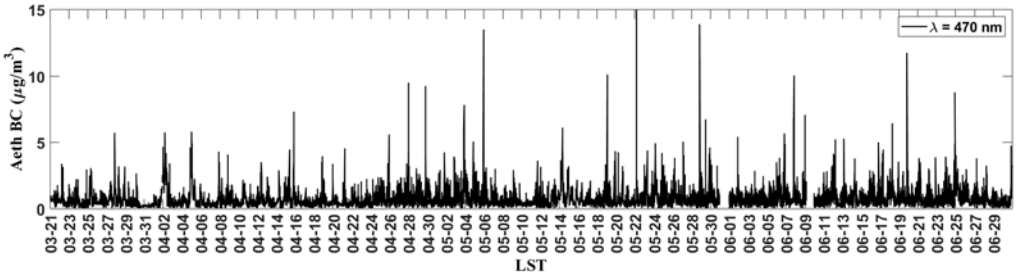

Figure 24. Aerosol BC concentrations ($\mu g/m^3$) measured at the 470 nm and reported as 5 min averages.

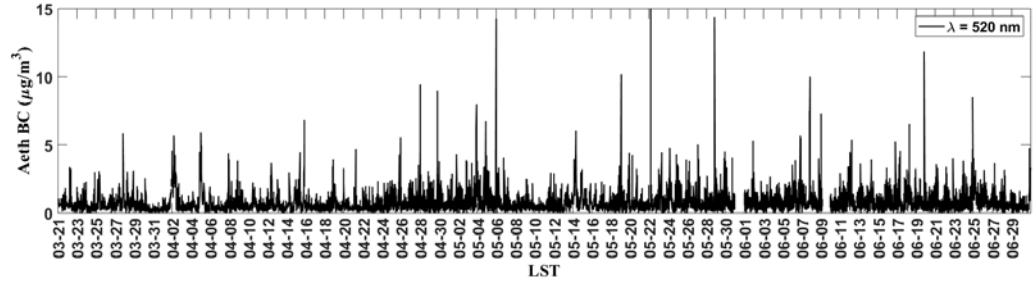

Figure 25. Aerosol BC concentrations (μg/m^3) measured at the 520 nm and reported as 5 min averages.

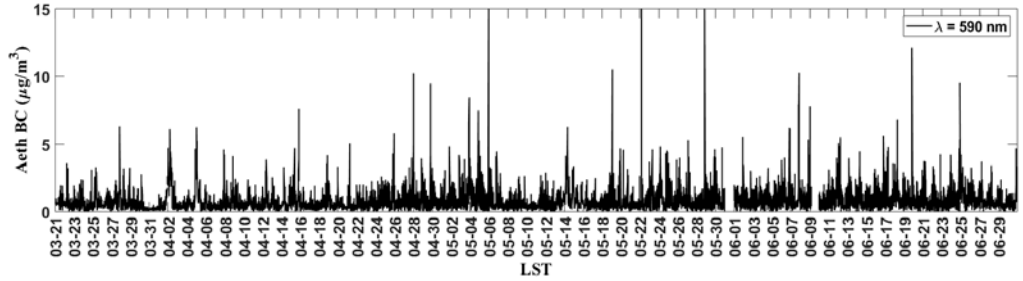

Figure 26. Aerosol BC concentrations (μg/m^3) measured at the 590 nm and reported as 5 min averages.

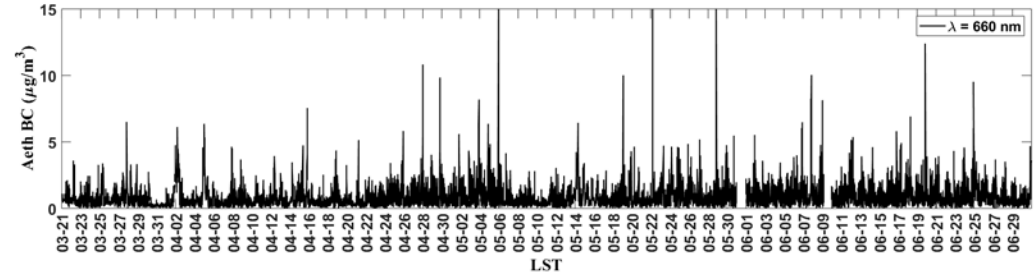

Figure 27. Aerosol BC concentrations (μg/m^3) measured at the 660 nm and reported as 5 min averages.

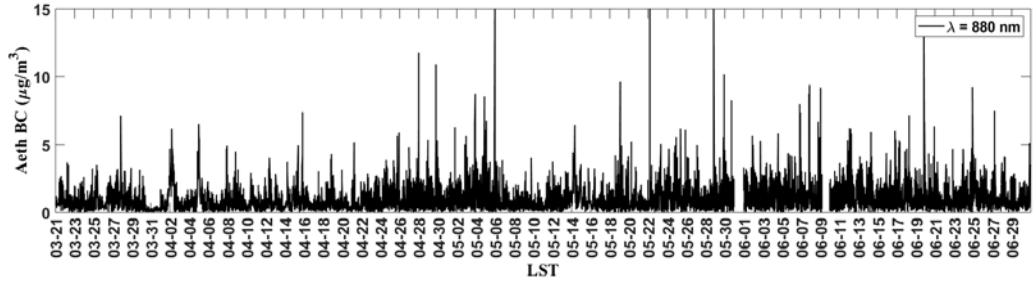

Figure 28. Aerosol BC concentrations (μg/m^3) measured at the 880 nm and reported as 5 min averages.

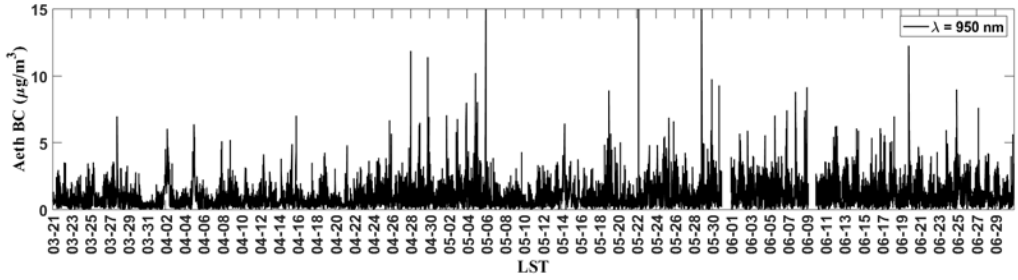

Figure 29. Aerosol BC concentrations (μg/m^3) measured at the 950 nm and reported as 5 min averages.

4.3.2 Aerosol Absorption Weekly Averages – Aethalometer

Figure 30, reports weekly averages of the aerosol ($PM_{2.5}$) BC concentrations (μg/m^3) measured at 880 nm using the aethalometer. The weekly average mass concentration of equivalent BC measured by aethalometer model AE42 is plotted in this figure. AE42 uses seven wavelengths to measure light attenuation, the sixth wavelength corresponding to 880nm is considered as the equivalent BC concentration.

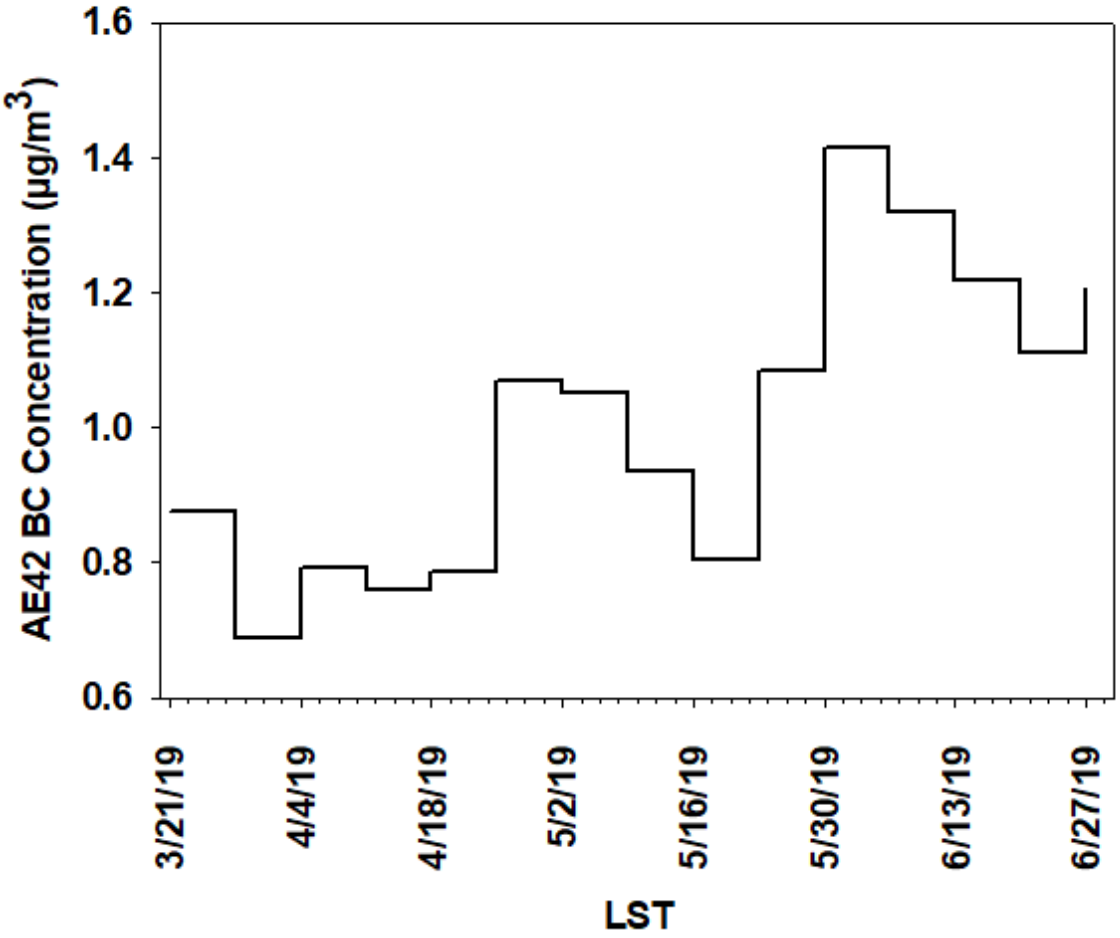

Figure 30. Weekly averaged aerosol BC concentrations (µg/m^3) measured at the 880 nm.

4.4 Trace gas Time Series Data – CO and NO_x

4.4.1 CO and NO_x five minute averages

Trace gas measurements for CO and NO_x were completed in the Baylor Air Quality Trailer to allow for calculation of enhancement ratios during biomass burning events, to understand diel variations, and to track seasonal trends. Both CO and NO_x had daily peaks in the morning and late evening.

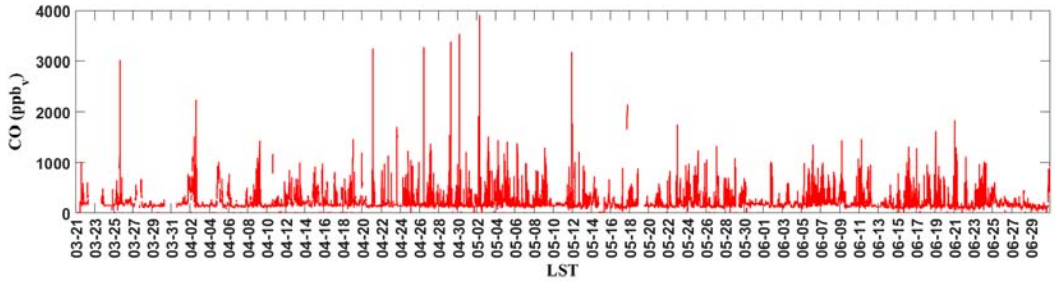

Figure 31. Atmospheric CO concentrations (ppbv) reported as 5 min averages.

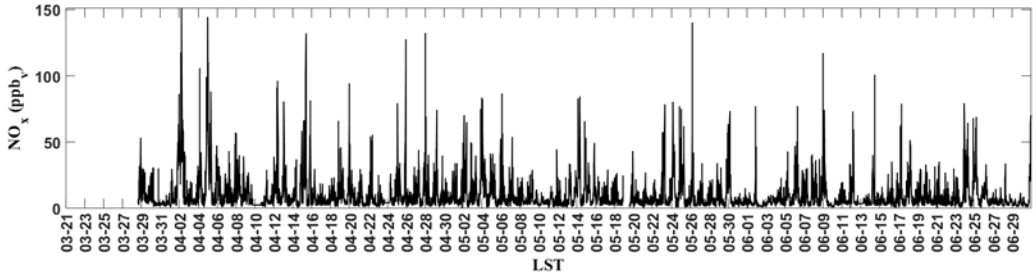

Figure 32. Atmospheric NO_x concentrations (ppbv) reported as 5 min averages.

4.4.2 CO and NO_x weekly averages

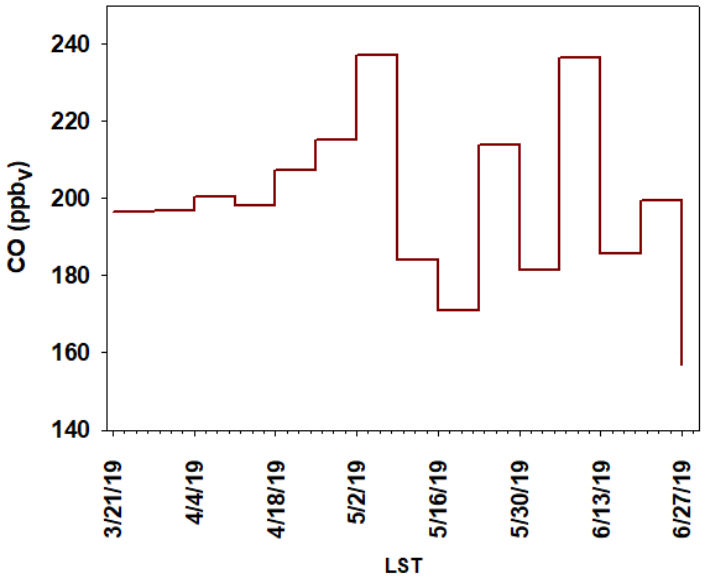

Figure 33. Weekly averaged atmospheric CO concentrations (ppbv).

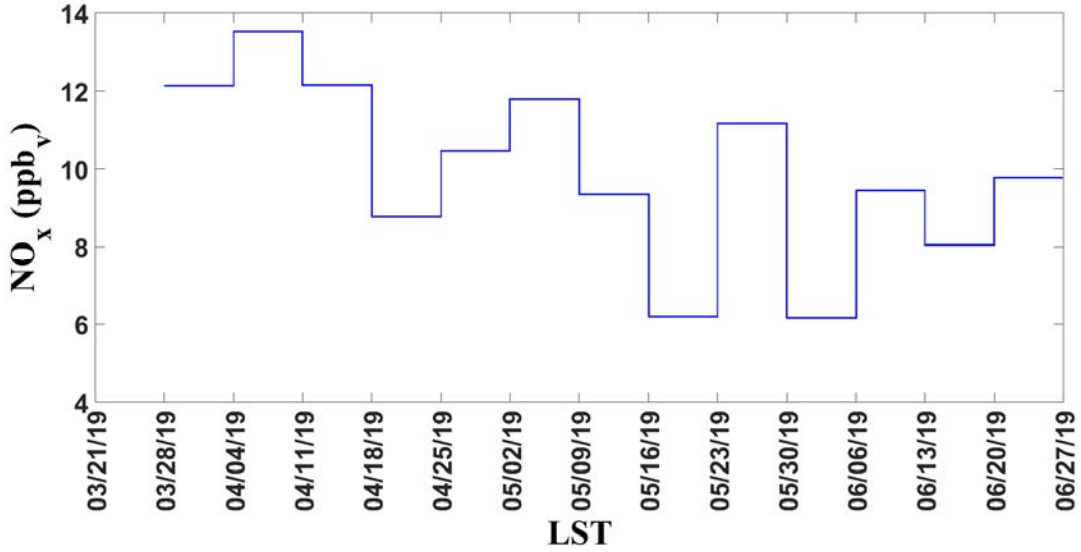

Figure 34. Weekly averaged atmospheric NO_x concentrations (ppbv).

4.4.3 Diel Variation in CO and NO_x

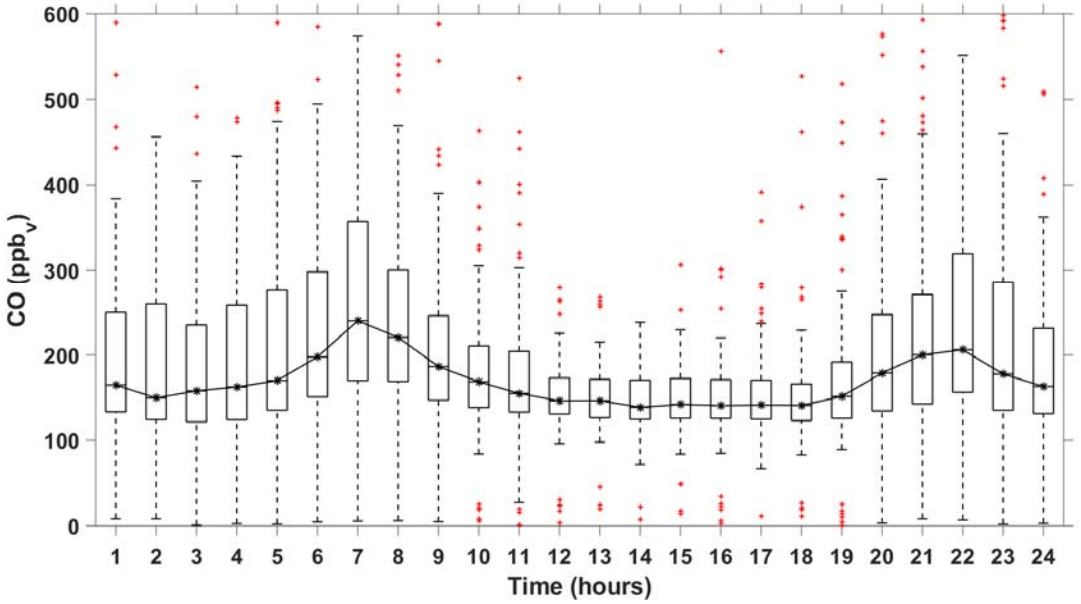

Figure 35. Diel variation in atmospheric CO concentrations (ppbv).

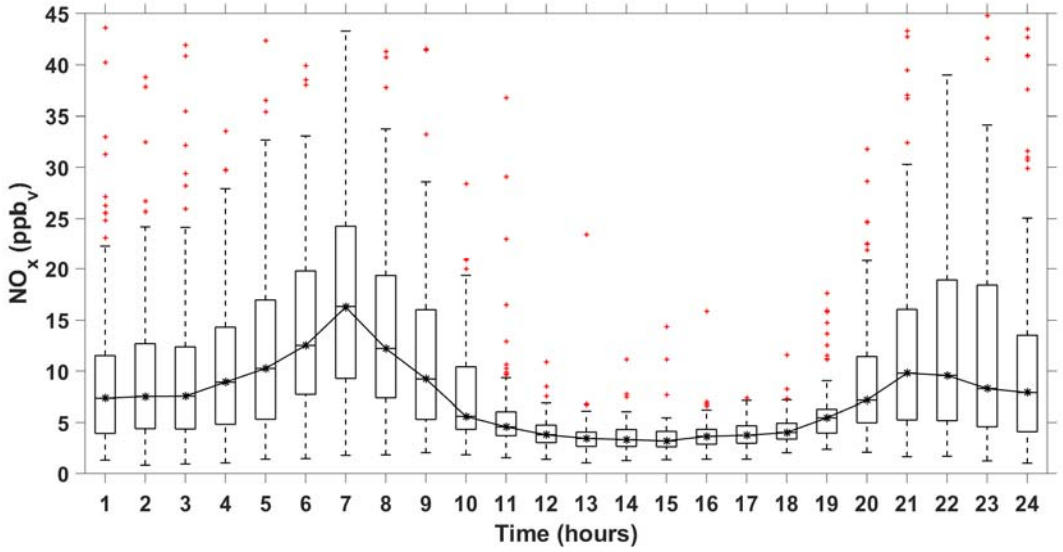

Figure 36. Diel variation in atmospheric NO_x concentrations (ppbv).

4.5 Enhancement Ratios – Weekly Averages

4.5.1 Aerosol absorption coefficient enhancement ratios

There is no distinct trend in the enhancement ratio for the three different TAP-based absorption coefficients with respect to (wrt) ambient CO concentrations. The NO_x enhancement ratio wrt CO does have a decreasing trend over the Mar – Jun campaign.

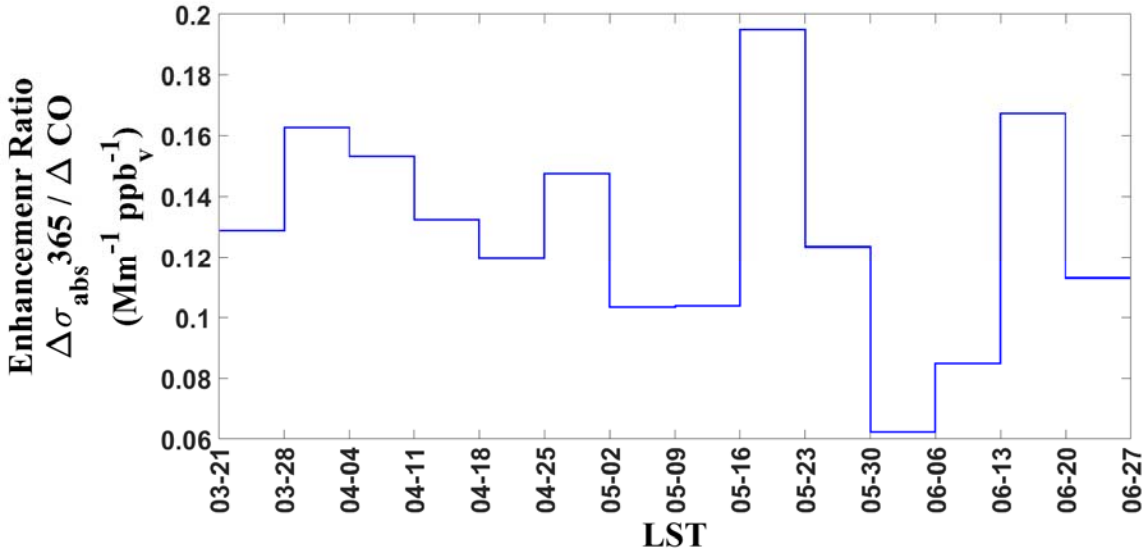

Figure 37. Weekly average enhancement ratios of TAP absorption coefficients (Mm^{-1}) measured at the 450 normalized to atmospheric CO concentrations (ppbv).

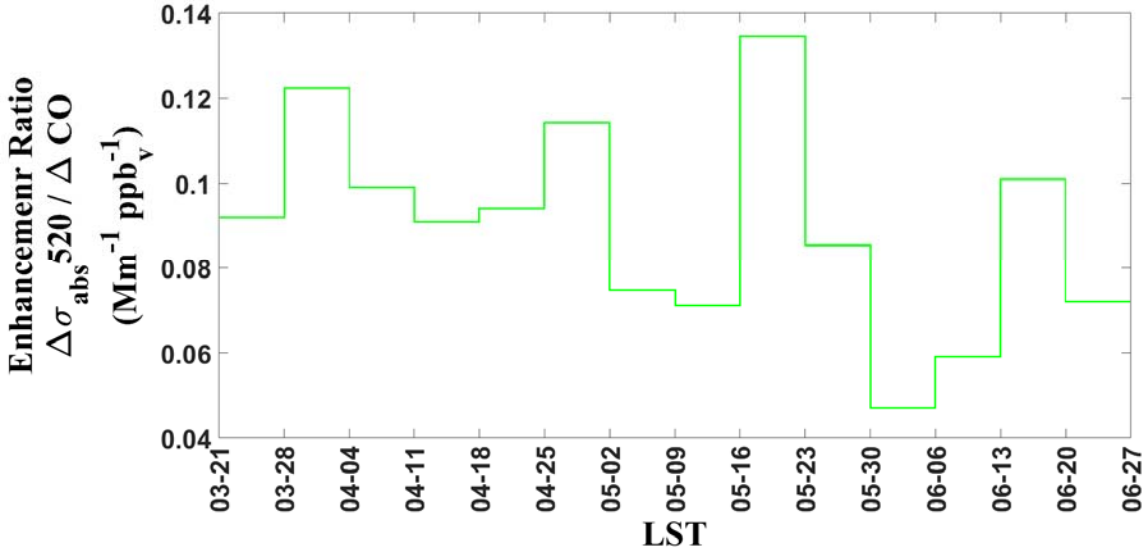

Figure 38. Weekly average enhancement ratios of TAP absorption coefficients (Mm^{-1}) measured at the 520 normalized to atmospheric CO concentrations (ppbv).

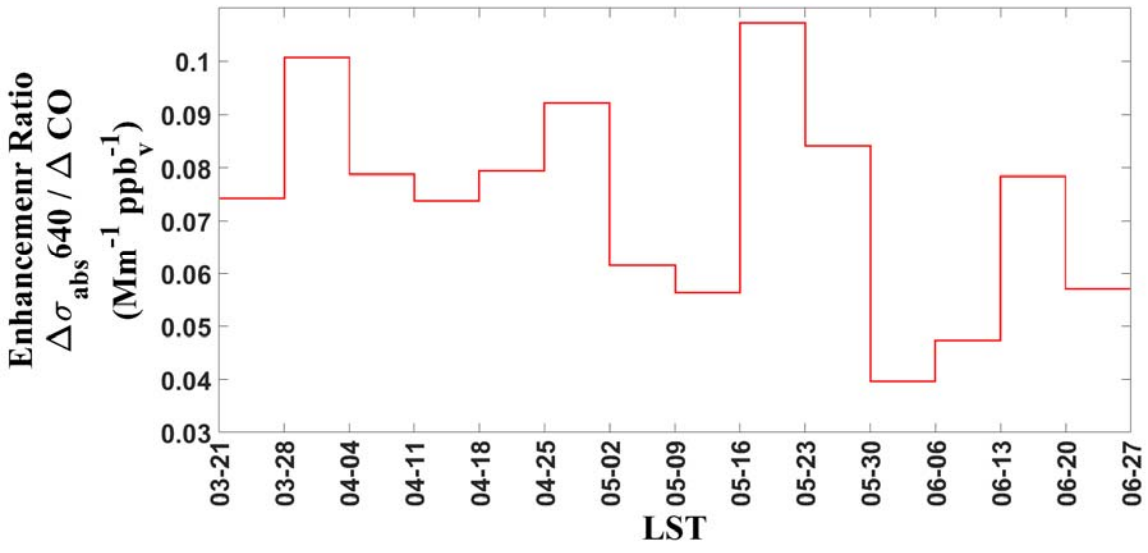

Figure 39. Weekly average enhancement ratios of TAP absorption coefficients (Mm^{-1}) measured at the 640 normalized to atmospheric CO concentrations (ppbv).

4.5.2 Aerosol scattering coefficient enhancement ratios

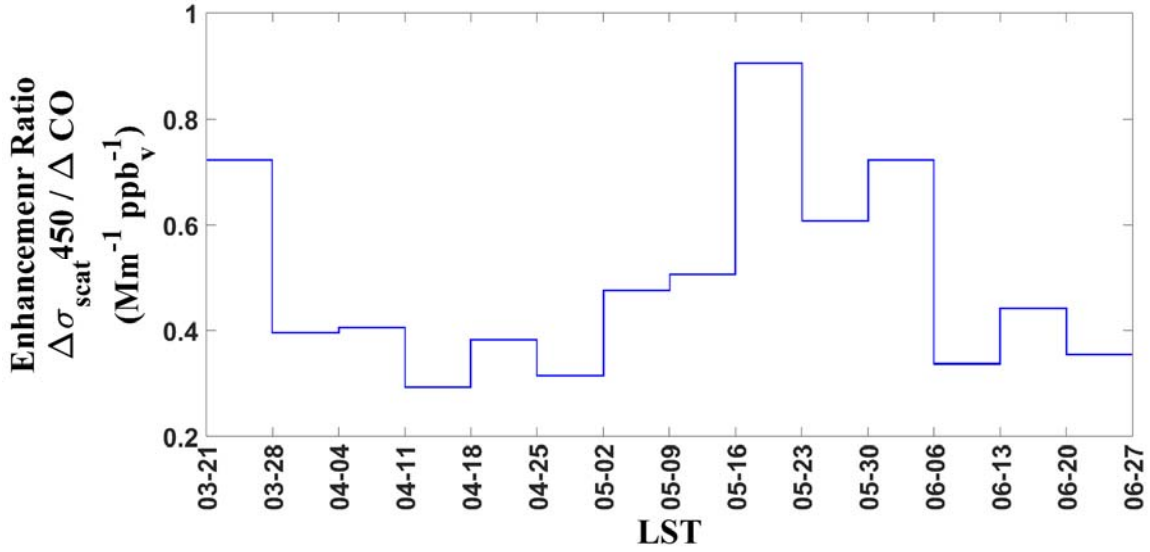

Figure 40. Weekly average enhancement ratios of nephelometer scattering coefficients (Mm^{-1}) measured at the 450 normalized to atmospheric CO concentrations (ppbv).

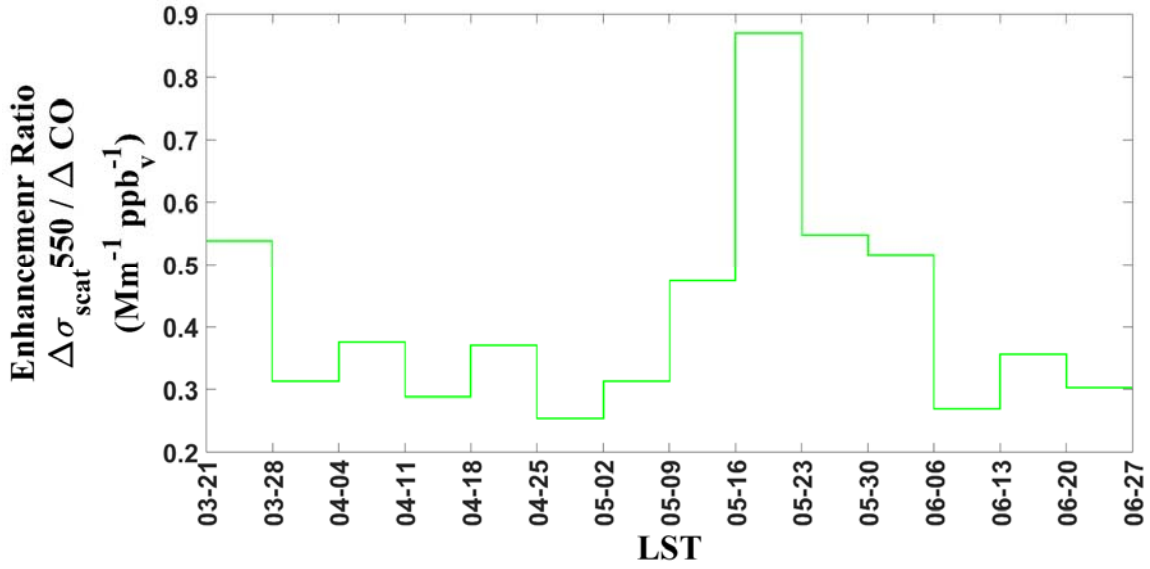

Figure 41. Weekly average enhancement ratios of nephelometer scattering coefficients (Mm^{-1}) measured at the 550 normalized to atmospheric CO concentrations (ppbv).

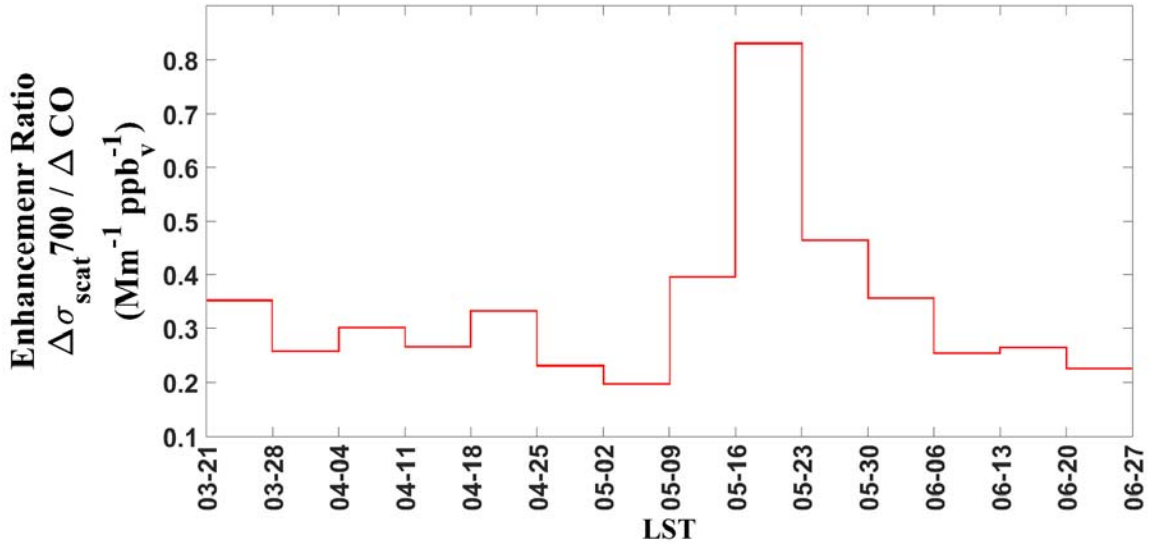

Figure 42. Weekly average enhancement ratios of nephelometer scattering coefficients (Mm^{-1}) measured at the 700 normalized to atmospheric CO concentrations (ppbv).

4.5.3 Aerosol absorption enhancement ratios – Aethalometer

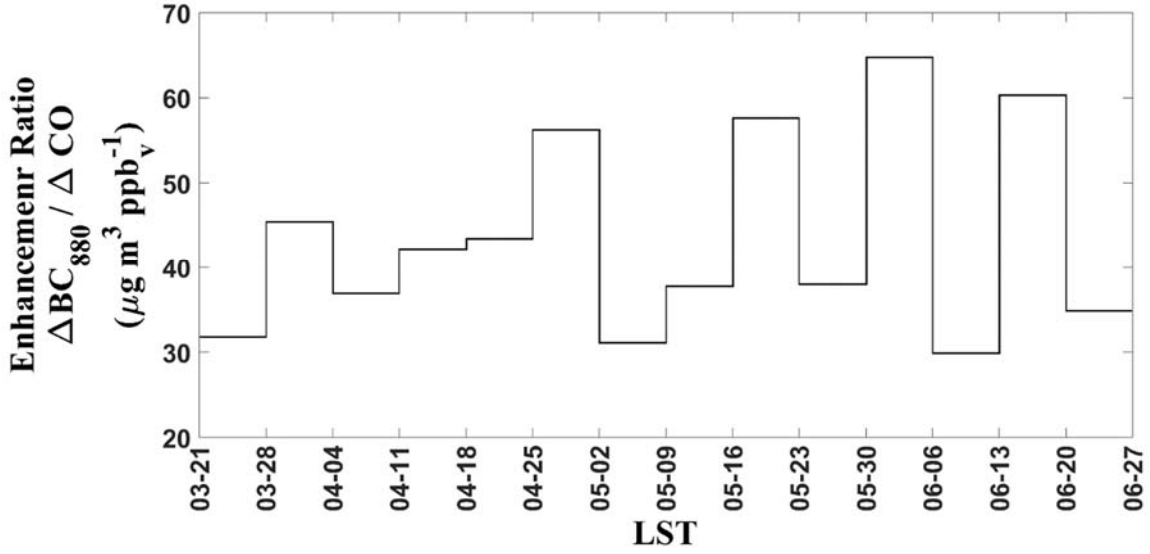

Figure 43. Weekly average enhancement ratios of aethalomter absorption coefficients (Mm^{-1}) measured at the 880 normalized to atmospheric CO concentrations (ppbv).

4.5.4 Trace gas enhancement ratios – NO_x

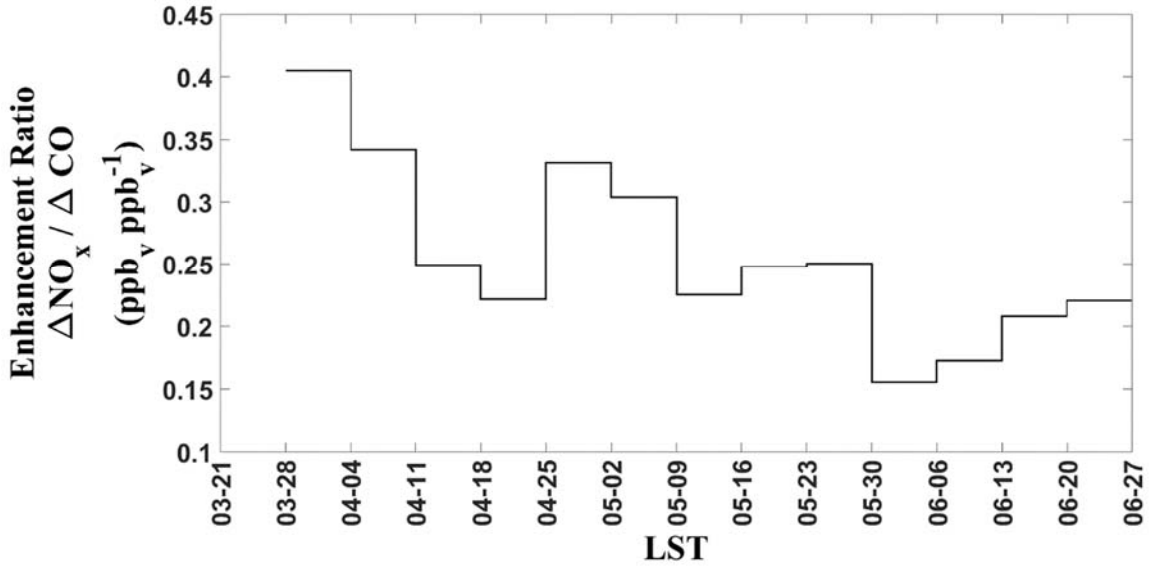

Figure 44. Weekly average enhancement ratios of atmospheric NO_x concentrations (ppbv) normalized to atmospheric CO concentrations (ppbv).

4.6 Biomass Burning and Dust Events

According to previous literature, BC emission from fossil fuel combustion is spectrally independent, thus has AAE value of 1 (Bergstrom et al., 2007). Therefore, the deviation of AAE from unity can be attributed to the additional light absorbing carbon or brown carbon from other sources like biomass burning (Bergstrom et al., 2002; Praveen et al., 2012; Srivastava et al., 2012). With high influence from the adjacent interstate highway, there is consistent contribution from motor vehicle exhaust on the absorbing aerosol at the UTEP site. This high impact is evident in the campaign mean AAE, 1.1 ± 0.17. An increase in the AAE from the average value would indicate a change in the sources of absorbing aerosols in El Paso. Therefore, a conservative cutoff of AAE = 1.2 has been assigned to separate the average urban combustion aerosol from biomass burning – influenced aerosol. In other words, AAE < 1.2 is considered BC dominated fossil fuel whereas AAE > 1.2 indicates influence from biomass burning or wildfires. Figure 45, a bar plot of the percent of weekly data points with AAE > 1.2 highlights the trend in increasing biomass burning contribution from Mar – June for this campaign. Based on personal communication with David Sullivan (University of Texas), our June peak matches a

peak in the average June contribution of the smoke/fire factor based on multi-year (2009-2016) positive matrix factorization source apportionment from filter-based speciation for El Paso (Chamizal site).

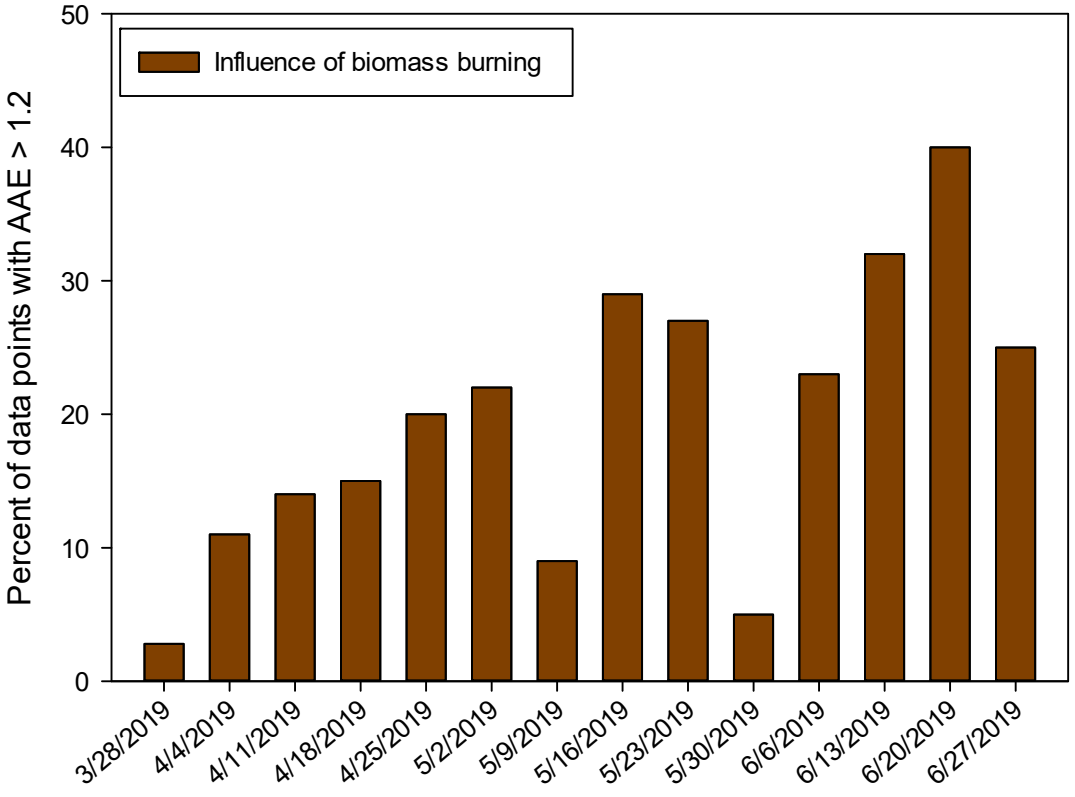

Figure 45. Assessment of the percentage of AAE values by week which indicate influence from biomass burning (AAE > 1.2). From the figure, we can infer that the week starting from June 20 to June 26 had highest contribution of biomass burning sources (p=40%) compared to other weeks.

As an example of the ability of the TAP + nephelometer combination to identify the influence of biomass burning, an event on June 23, 2019 will be described in detail. Influence of biomass-burning event at the site was identified with two distinct periods occurring on June 23, 2019 (Figure 46) of elevated AAE. These periods had AAE > 1.2. MODIS fire maps during that period identified fires upwind in both Arizona and Mexico (Figure 47). HYSPLIT back trajectories modeled plume transport from the source regions to the $(BC)^2$ El Paso site (Figure

48). However, it is apparent from the BTs and the NOAA smoke product that El Paso was on the edge of these biomass burning plumes.

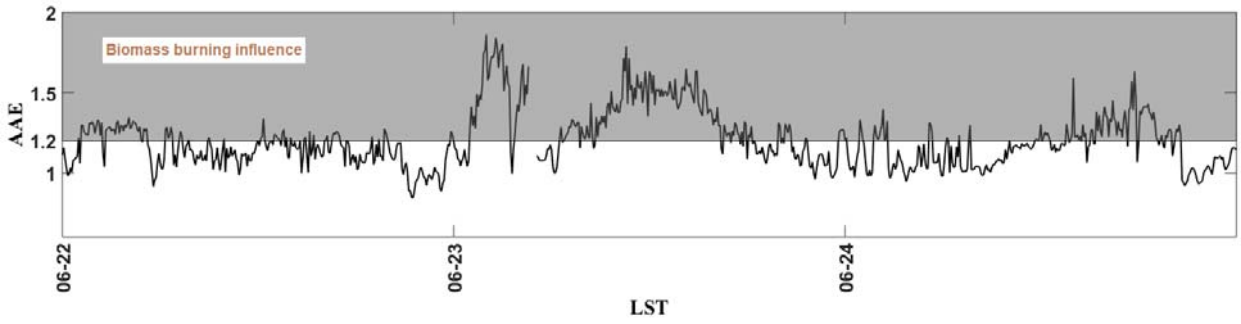

Figure 46. Aerosol absorption Ångström exponent 5 min averages for June 22-24th, 2019. The grey box designates AAE > 1.2 AAE.

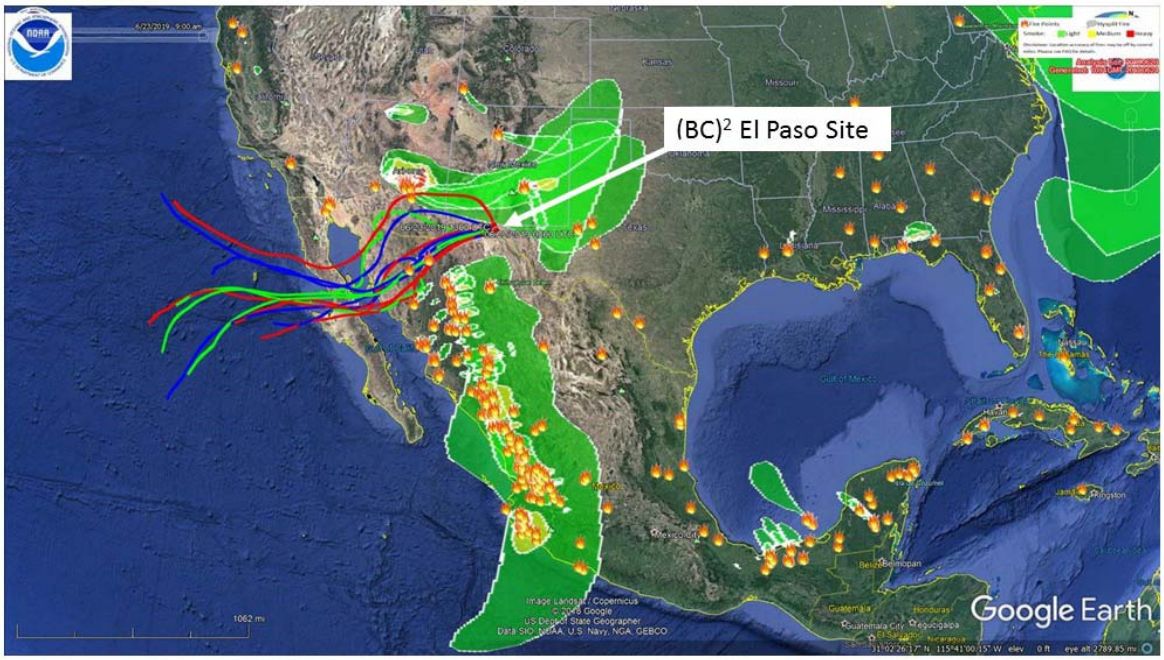

Figure 47. NASA's MODIS active fire detection map overlaid with modeled plume transport and HYSPLIT back trajectories.

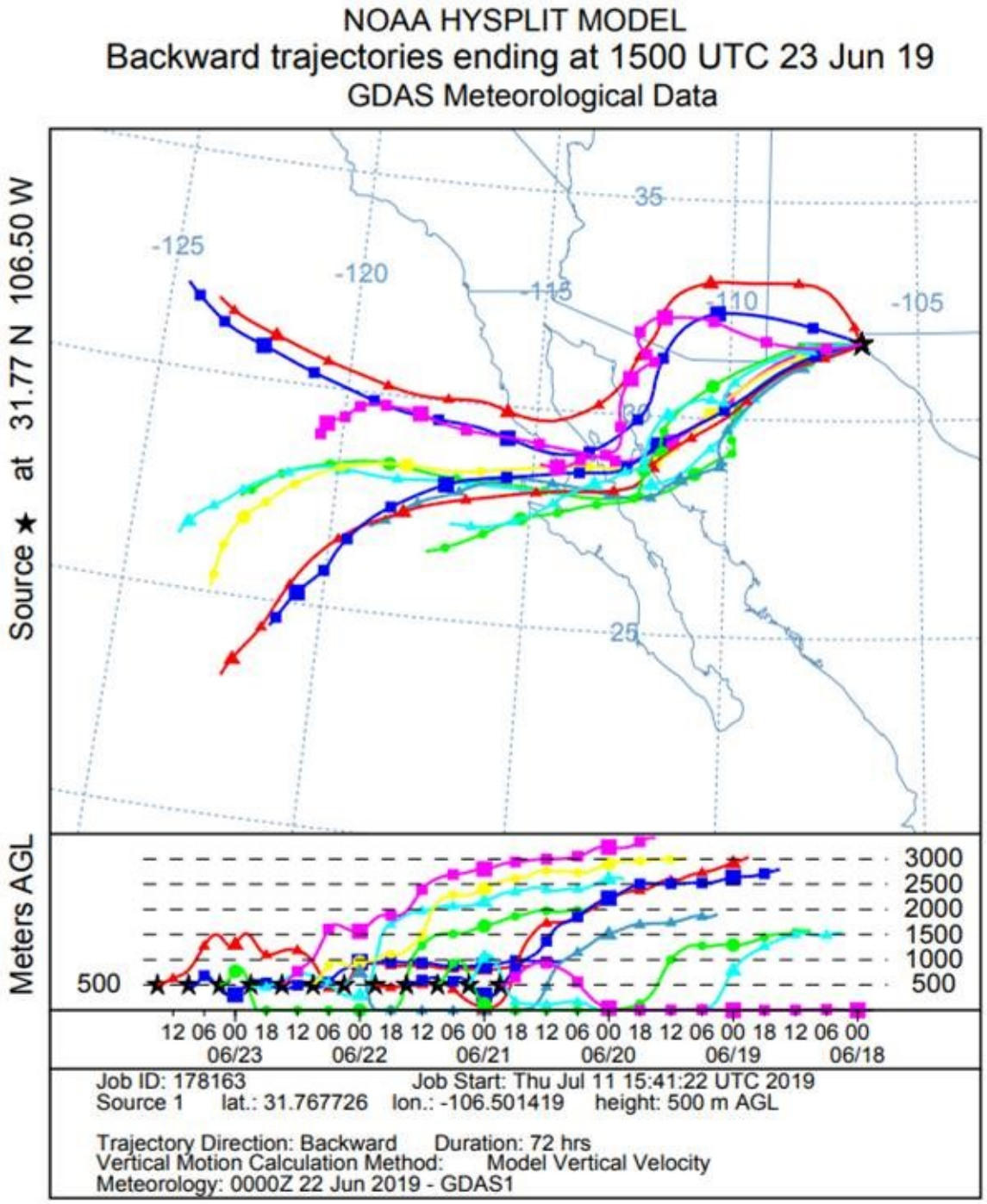

Figure 48. NOAA HYSPLIT three day back trajectories for June 23 to the $(BC)^2$ El Paso site.

To improve the assessment and identification of a biomass-burning event and reduce the overall number of assumptions, the AAE can be plotted against the SAE. Thereby allowing for

the simultaneous examination of both types of optical properties (specifically absorption and scattering). Figure 49, plots AAE vs SAE for the entirety of the campaign and highlights potential biomass-burning events, specifically when the AAE increases above 1.2 while the SAE remains relatively low.

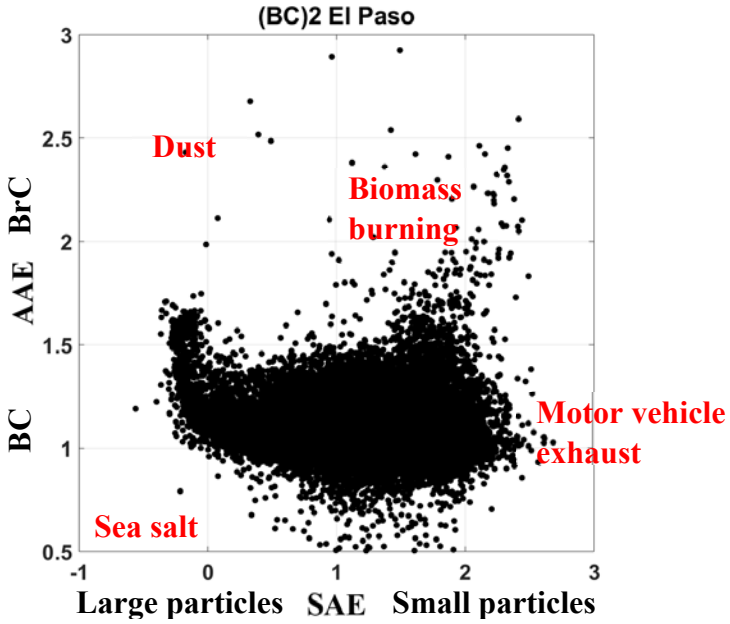

Figure 49. AAE vs SAE for the entire campaign with rough demarcations of source and aerosol type based off the aerosol classification matrix from Cappa et al. (2016).

To illustrate how the combination of AAE and SAE can uniquely identify biomass burning versus dust events. The biomass burning event identified in Figure 50 on 6/23 is compared to the campaign average and also a dust event identified on 4/10 (this event corresponds with peak hourly $PM_{2.5}$ of 116.7 ug/m^3 and PM_{10} of 980 ug/m^3 from TEOM at the TCEQ CAMS 12 site collocated at UTEP).

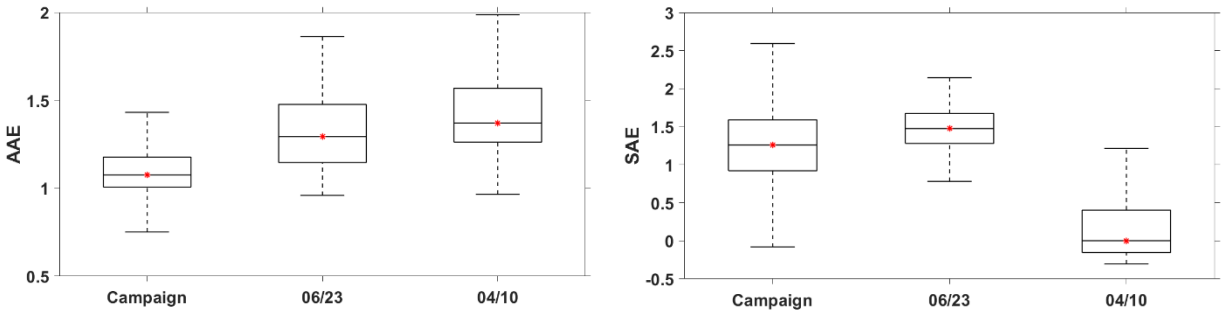

Figure 50. Box and whisker plots of the median AAE (left) and SAE (right) for the campaign average, 6/23 and 4/10 days.

Based on the classification scheme in Figure 49, it is clear that 6/23 has biomass burning impact with higher AAE, while 4/10 has a dust signal of higher AAE and low SAE. Since the 6/23 event was not continuously impacting for the full 24 h period and was on the edge of the plume (Figure 47), the enhancement in the AAE signal is significant, but not extreme. However, as evidenced by the extreme increase in $PM_{2.5}$ and PM_{10}, the 4/10 dust event temporarily overwhelmed the urban signal and both the AAE and the SAE show a greater deviation from the campaign average.

To evaluate whether SAE < 0 could reveal seasonality to dust events in El Paso, this cutoff has been applied to plot weekly dust influence on scattering aerosol in El Paso (Figure 51). Unlike the AAE, there is no long term trend, but weeks with high influence. These periods would need to be further investigated to determine the extent of dust impacts, however, the 4/10 event is clearly apparent in the weekly plots

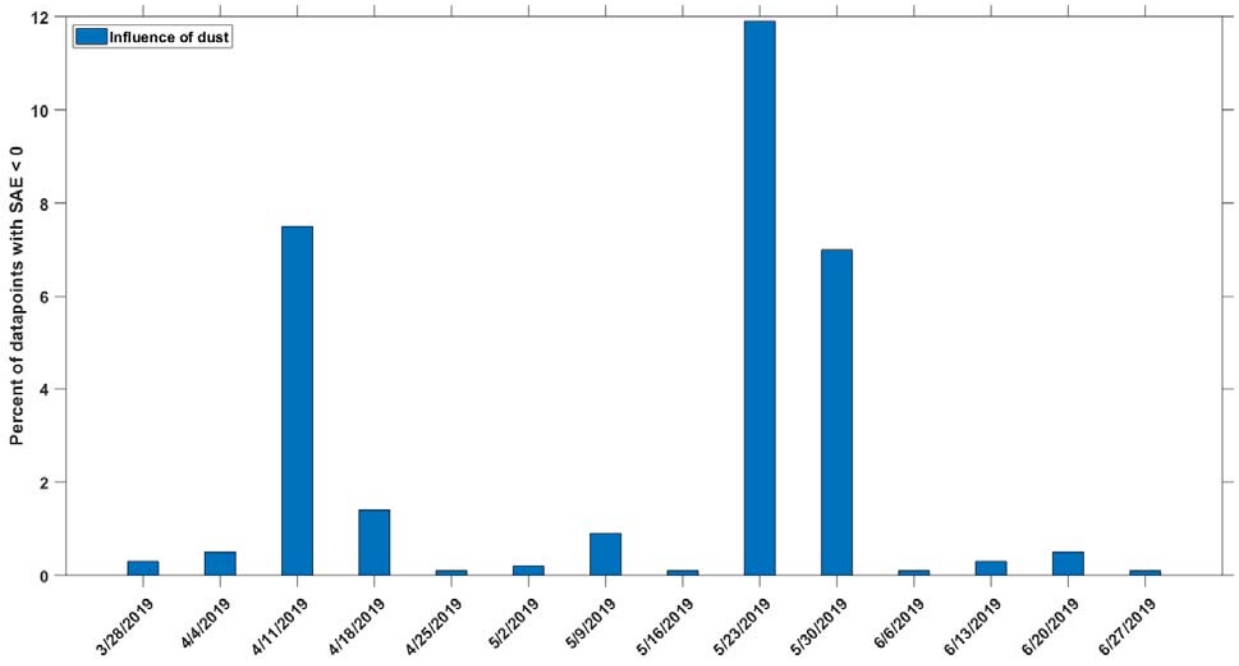

Figure 51. Weekly percent of data points with SAE < 0, an indicator of large particle influence.

This biomass-burning event was observed using two different optical measurements (absorption and scattering). CO, NO_x, $PM_{2.5}$, and PM_{10} had a diminished ability to observe the

biomass-burning event, Figure 52 – 54, respectively. CO, NO_x, $PM_{2.5}$, and PM_{10} data were acquired from the TCEQ CAMS 12 (UTEP) site (June 22-24, 2019).

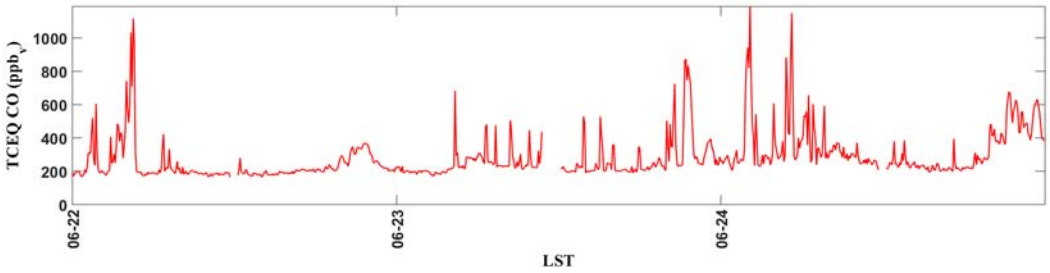

Figure 52. Atmospheric CO (ppbv) concentrations collected from the TCEQ CAMS 12 (UTEP) site (June 22-24, 2019) and reported as 5 min averages.

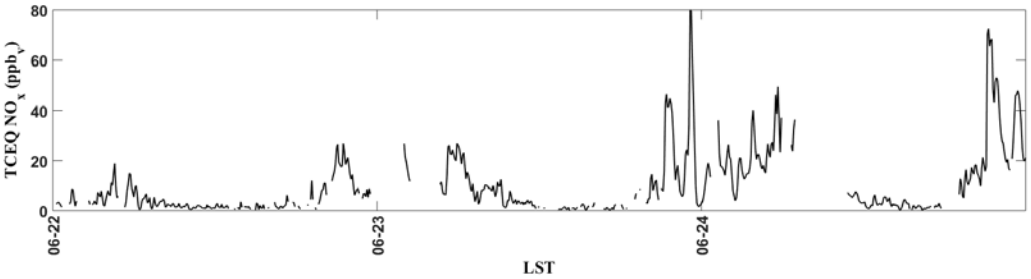

Figure 53. Atmospheric NO_x concentrations (ppbv) collected from the TCEQ CAMS 12 (UTEP) site (June 22-24, 2019) and reported as 5 min averages.

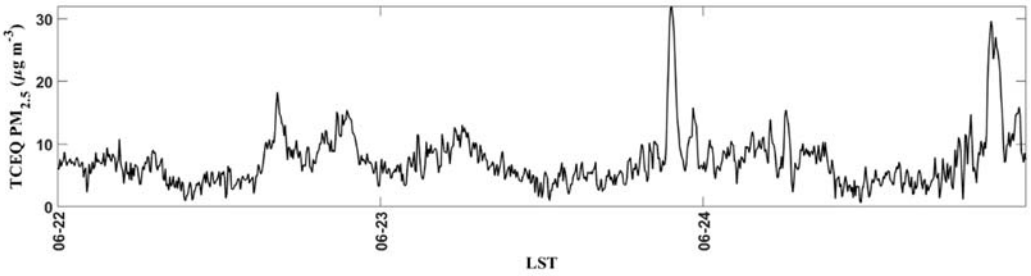

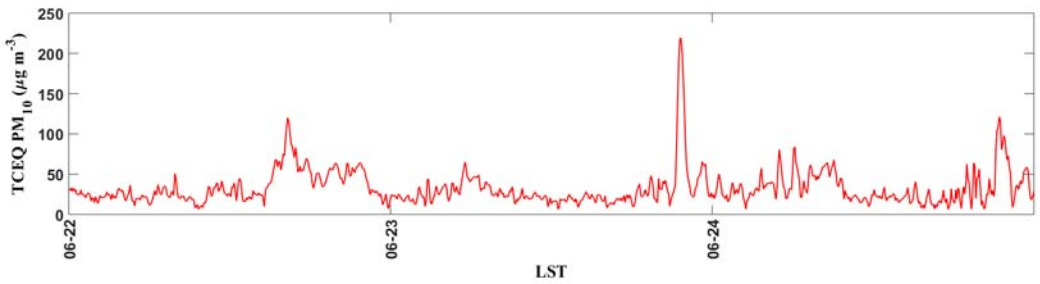

Figure 54. Atmospheric $PM_{2.5}$ and PM_{10} concentrations (top and bottom, respectively, μg m^{-3}) collected from the TCEQ CAMS 12 (UTEP) site (June 22-24, 2019) and reported as 5 min averages.

4.7 TAP evaluation

An in-depth evaluation of the TAP, suggest the TAP is capable of providing continuous and long-term aerosol absorption measurements (i.e. months) for the characterization of BC and BrC from biomass burning. The TAP provided the necessary sensitivity to identify the influence of a biomass-burning event, even within the confines of a large urban landscape and close proximity to a major interstate (i.e. I-10). Specifically, the AAE normalization improved the overall sensitivity of the observation (over absorption coefficients). This was not possible using other types of instrumentation including atmospheric concentrations of CO, NO_x, $PM_{2.5}$, or PM_{10}.

The TAP's relatively small footprint (space, power, and flowrate) would allow a TAP instrument to be housed within the confines of most air-monitoring site with limited site modification. The TAP is also equipped to handle a computer interface, which allows for offsite data storage and virtual or offsite monitoring. Depending on the ambient aerosol concentrations, the TAP would require a filter change every three days. This can be increased to six days with modified observations or the use of multiple TAP instruments. The two TAP instruments provided a strong agreement with each other (see section 6) and overall provided a high level of reproducibility. During the campaign (March 21st through June 30), the two TAP instrument required 2 hours or less of downtime due to maintenance that was not associated with filter changes.

A comparison of the TAP data with the AE42 data reveals a distinct improvement in instrument noise: the TAPs have a smooth data stream for the campaign, while the AE42 has much greater noise for the same period (see Figure 55 below).

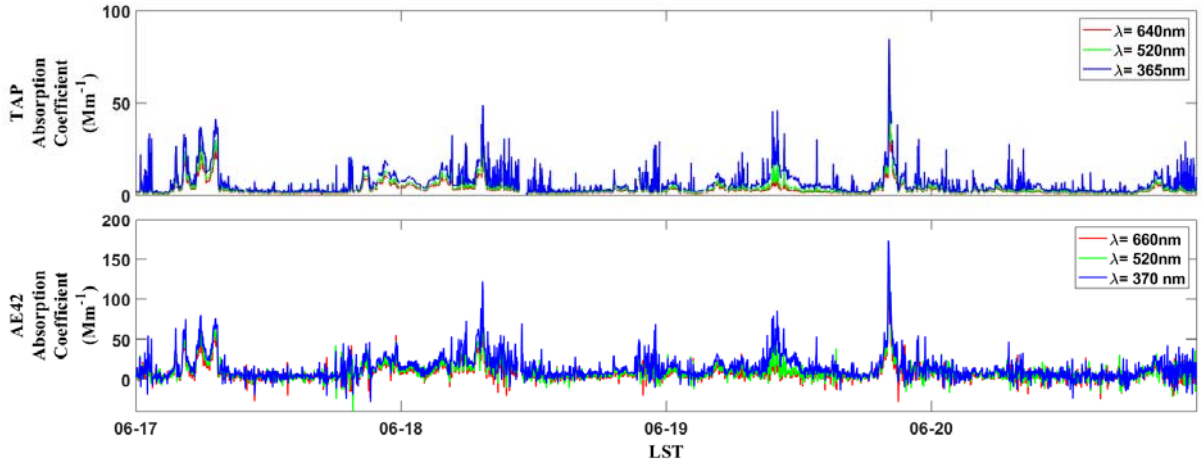

Figure 55. Comparison between the aerosol absorption coefficient (Mm^{-1}) measured using TAP (Top) and AE42 (Bottom) (5 min averages).

A comparison of the calculated AAE between the TAP and the AE42 required averaging the AE42 aethalometer data for 1 hour to minimize errors due to noise. At the hourly resolution, the two instruments had good correlation for the calculated AAE for June 17 -20, which had higher biomass burning influence. The TAP had a higher AAE than the AE42 for this period (Figure 56).

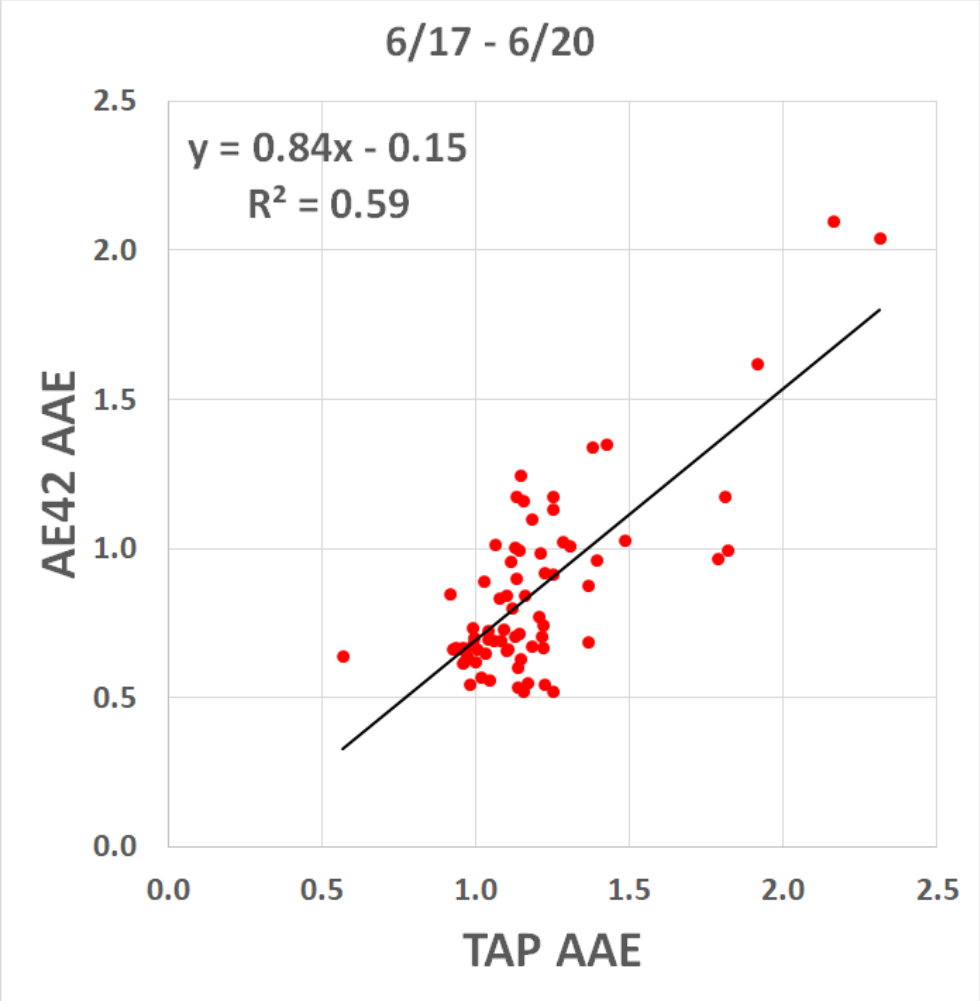

Figure 56. Correlations between the AAE measured using the TAPs and AE42 (5 min averages; June 17th through 20th).

4.7.1 Time and effort associated with the TAP

Time and effort associated with operating the TAPs and nephelometer during the campaign was assessed including training, daily checks, weekly onsite checks, consumables, and monthly checks (Table 1). Daily checks utilized TeamViewer to monitor instrumentation status and data acquisition. During the daily checks, real-time aerosol optical properties were plotted in daily plots. Furthermore, optical data was continuously uploaded to an external server, which served as a backup for site computer. Daily checks also included using internal cameras to visually inspect the trailer, instrumentation, and cylinder gases. Support personnel from the UTEP campus helped inspect the trailer and instrumentation weekly and performed routine

maintenance such as TAP filter changes. At least once a month, project personnel inspected the trailer and instrumentation during an on-site visit. The AE42 was not online and requires data to be downloaded manually every week. Table 1 also includes the average down time and frequency associated with filter changes, filter advancements, and calibrations. Table 1 does not include fraction of data omitted due to instrument noise on the AE42.

Table 1. Time and effort associated with the training and operation of the $(BC)^2$ El Paso trailer.

	Training (hr)	Time on site (hr)	Frenquence of Filter Changes / Advancements / Calibration	Time Gaps in Data (hr)	Weekly Remote Operation (hr)
TAP	2	1/wk	7±1 days	1/wk	2-3
Nepthelometer	2	0.5/2wk	15±1 days	0.5/2wk	2-3
Aethalometer	2	0.75/wk	3±1 days	0.75/wk	-

4.7.2 Co-located instrumentation requirements

Within the scope of this project, the PIs investigated what instrumentation would be needed for BrC and AAE monitoring. The TAP and nephelometer combination provided the most useful data for identification of biomass burning plume influence. However, in this campaign El Paso was on the edge of plumes, so it is not clear whether the CO and NO_x were as affected by the plume. Co-location with $PM_{2.5}$ and PM_{10} was helpful in identifying the impact of dust plumes in the April 10 event.

5.0 Data Audits and Quality Assurance

5.1 Aerosol absorption – TAP A and TAP B

5.1.1 Data Audit

As part of the project's design to provide a 10% data quality audit, key instruments were deployed in duplication or co-location with instruments associated with the TCEQ CAMS 12 (UTEP) site. TAP A and TAP B were operated simultaneously for over 12 days (greater than 10%) throughout the campaign (Figure 57-59). This allowed for the direct comparison of aerosol absorption between the two TAPs instrumentation (i.e. TAP A and TAP B) for a wide

range of absorption coefficients. Modeling the relationship using a simple linear regression analysis allows for a quick and accurate assessment of the data (greater than 10% for each wavelength). The regression analysis shows strong correlations between the two instruments (for all three wavelengths), with r^2 greater than 0.98 and a slope of 0.96 (i.e. nearly 1). The derived AAE data from TAP A and TAP B was also examined using a linear regression model and show a strong agreement between the two instruments (r^2 greater than 0.93 and a slope of 0.98; Figure 60).

5.1.2 Completeness, precision, and accuracy.

Using the two TAP instruments, the completeness of the aerosol absorption measurements for the campaign was greater than 99.9 percent. Correlation plots (Figure 57-60) also suggest a high level of precision and accuracy between the two instruments. With the co-located data, it can be seen that there is a high degree of comparison, however, there are time series with an offset in slope between the two instruments. With the co-located data collected in this campaign, it is not clear what conditions result in this small change. There are very small differences between the flow rates for each instrument that do fluctuate independently over time (< 1% difference in flow rate). This may be contributing to the small difference in slope (figure inset for Figure 58), but more work is needed to understand why this small difference occurs. This difference is not sufficiently large to bias the ambient results.

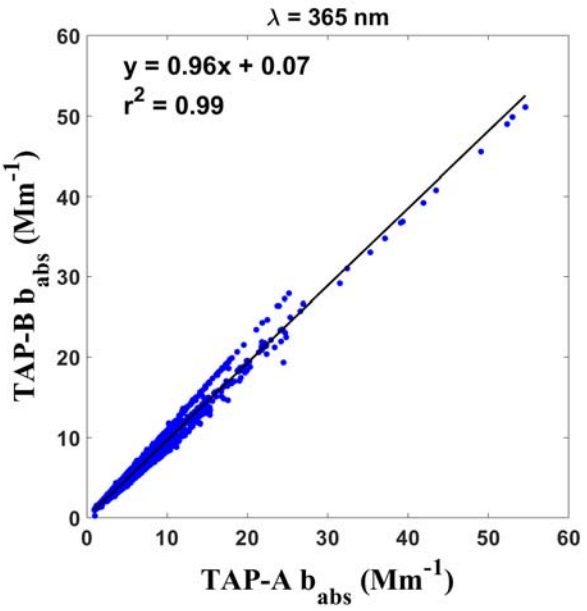

Figure 57. Correlations between the aerosol absorption coefficient (Mm^{-1}) measured at 365 nm using TAP A and TAP B (5 min averages).

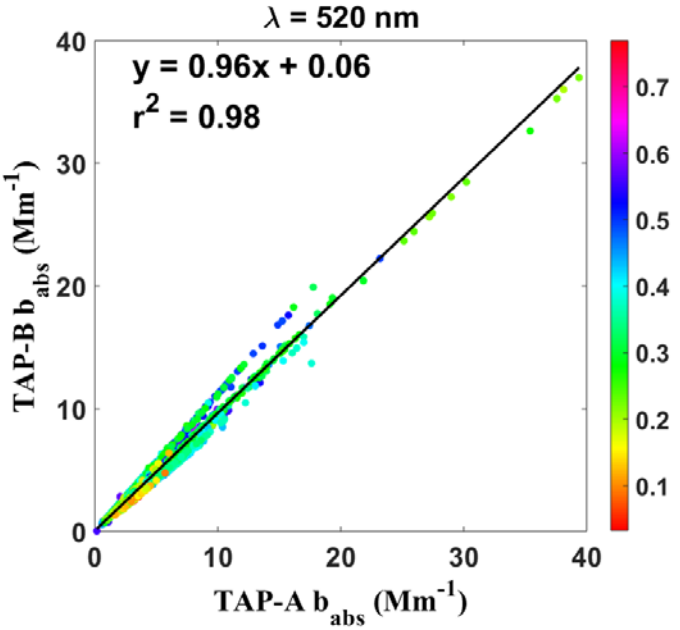

Figure 58. Correlations between the aerosol absorption coefficient (Mm^{-1}) measured at 520 nm using TAP A and TAP B (5 min averages). The % difference in flow rate between the two taps is the color scheme used for the data points.

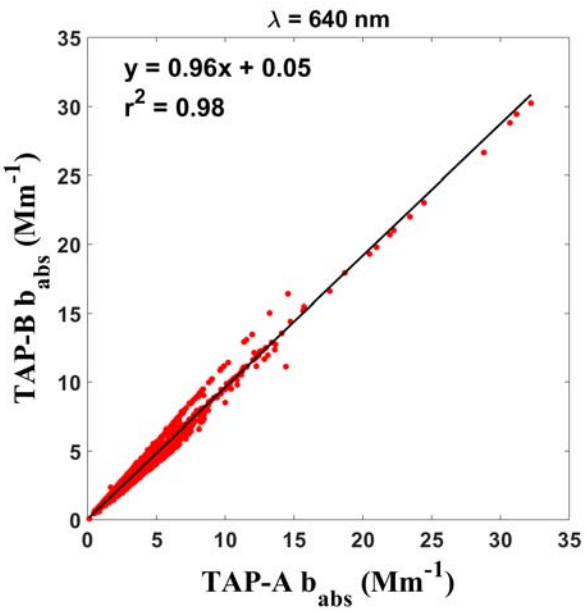

Figure 59. Correlations between the aerosol absorption coefficient (Mm^{-1}) measured at 640 nm using TAP A and TAP B (5 min averages).

Figure 60, reports the relationship between AAE between the two TAPs. AAE were calculated using aerosol absorption coefficient (Mm^{-1}) for 365, 520, and 640 nm in equation 7 and. The slope and r^2 were near 1.

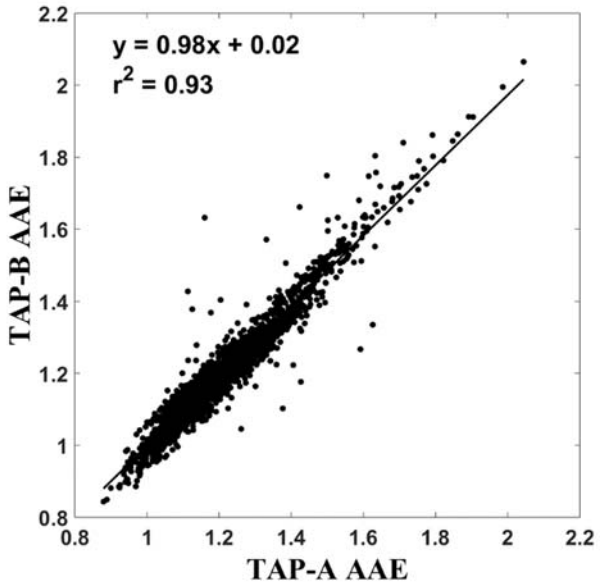

Figure 60. Correlations between the absorption Ångström exponent calculated for TAP A and TAP B (5 min averages).

5.2 Aerosol Scattering – Nephelometer

5.2.1 Data Audit

To fulfill the 10% required data audit, nephelometer total scattering data measured during the entire campaign was corrected for angular truncation using Anderson and Ogren (2007) method for all three wavelengths (Figure 61-63). The coefficient of determination (r^2) between the true total scattering coefficient and uncorrected scattering coefficients is 0.99 for 700 nm and 0.98 for both 450 and 550 nm wavelengths. However, the slope of the linear regression shows that the uncorrected total scattering is around 25%, 25% and 23% lower than the corrected total scattering in 700, 550 and 450 nm respectively. The observed bias in present measurement is in the range as reported by Moosmuller and Arnott (2003).

5.2.2 Completeness, precision, and accuracy.

The completeness of the atmospheric scattering measurements for the campaign was greater than 99.9 percent. The deviation of the slope from 1 (Figure 61-63) suggest a reasonable level of precision and accuracy in the observed (ranges reported by Moosmuller and Arnott (2003).

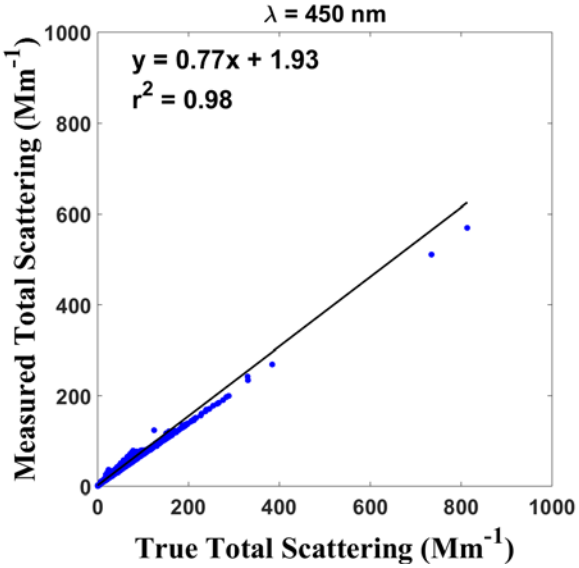

Figure 61. Total scattering vs scattering corrected for angular truncation using Anderson and Ogren (2007) method for 450 nm.

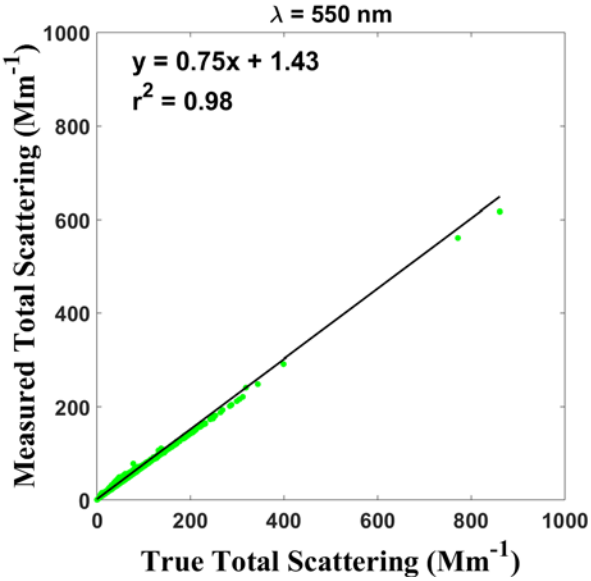

Figure 62. Total scattering vs scattering corrected for angular truncation using Anderson and Ogren (2007) method for 550 nm.

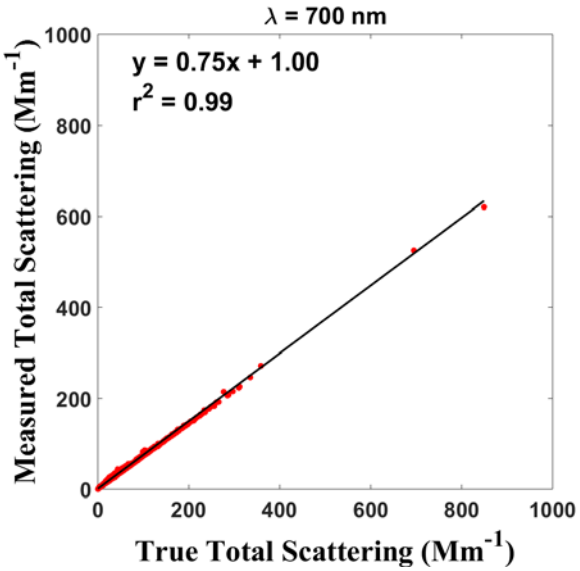

Figure 63. Total scattering vs scattering corrected for angular truncation using Anderson and Ogren (2007) method for 700 nm.

5.3 Trace Gases – CO and NO_x

5.3.1 Data Audit

The CO and NO_x instrumentation were co-located with instrumentation associated with the TCEQ CAMS 12 (UTEP) site and as such represent an opportunity to fulfill the quality assurance requirements of a 10% data quality audit. The 5 minute averaged CO (Figure 64) and NO_x (Figure 65) data from TCEQ CAMS12 site and our measurements were compared and the correlation is plotted in the figure below. NO_x was calculated as the sum of the NO and NO_2 measurements. As a part of QAQC, the data from our measurements during span calibration, zeroing and whenever the instrument had fault were removed prior to comaprison. We used orthogonal linear regression to comapre the two sets of measurements. Unlike standard regression which assumes only the dependent variable has error, the orthogonal regression assumes possibility of errors in both variables x and y variable (Leng et al., 2007). In our case, as we are not certain that one of the two measurements is free of error, we chose to use the orthogonal linear regression. The orthogonal regression, however, doesn't calculate the r^2 value. Since the datapoints are close to the regression line for both CO and NO_x indicates that's the the two sets of measurements are comparable.

5.3.2 Completeness, precision, and accuracy.

The completeness of the atmospheric CO and NO_x measurements for the campaign was greater than 99.9 percent. Correlation plots (Figure 64-65) also suggest a high level of precision and accuracy between trace gas instrumentation at the $(BC)^2$ El Paso site and the TCEQ CAMS 12 (UTEP) site.

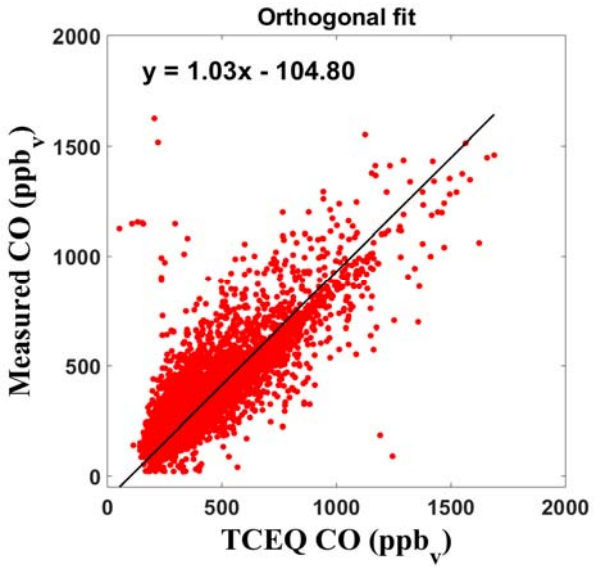

Figure 64. Correlation plots comparing CO measurements from $(BC)^2$ El Paso with CO data measured at the TCEQ CAMS 12 UTEP.

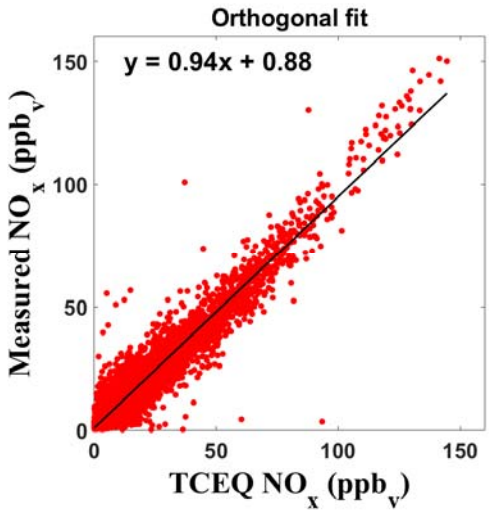

Figure 65. Correlation plots comparing NO_x measurements from $(BC)^2$ El Paso with NO_x data measured at the TCEQ CAMS 12 UTEP.

6.0 Conclusions

The PIs successfully conducted a long-term field campaign, where a suite of small footprint, low power, low maintenance, optical instruments was deployed in El Paso, TX from March to June 2019. Project PIs constructed a portable air monitoring trailer capable of remotely assessing BB event in urban centers across Texas. Instrumentation deployed included two, three wavelength TAPs, a three wavelength nephelometer, and a seven channel aethalometer. Absorption and scattering measurements were conducted on $PM_{2.5}$. Variability in absorption and scattering coefficients highlighted the complexity of optical measurements in an urban atmosphere, where the urban signal is dominated by high temperature combustion (e.g., motor vehicle exhaust). Variability with in these optical measurements was dramatically reduced by calculating AAE and SAE from the absorption and scattering coefficients, respectively.

AAE was relatively stable for most of the campaign with values near 1. An AAE of 1 was used as the baseline values and represented the El Paso urban atmosphere. Baseline AAE and SAE values were used to identified period of influence from dust and biomass burning. AAE values greater than 1.2 with durations of 2 hrs or more were used to identified potential biomass-burning events. The 1.2 threshold was determined using one standard deviation greater

than the Mar-Jun $(BC)^2$ El Paso campaign mean. During this campaign, June was the most impacted month of the campaign with over five potential biomass-burning events identified. It is important to note, that during this period of elevated AAE values, the SAE also increased which indicates smaller particle sizes.

Remote sensing data was acquired from federal databases and was used to assess the feasibility of smoke from known fires on El Paso. Remote sensing data included data from NASA MODIS Active Fire Data, NOAA Hazard Mapping Smoke Product, and NOAA HYPLIT 72-hr back trajectory. Remote sensing data was layered onto a regional map using Google Earth. Smoke plumes and back trajectories from known fires with the region to El Paso, supported the identification of biomass-burning events using the TAPs. The elevated AAE values with accompanying remote sensing data, suggest that the TAP is well suited at identifying biomass-burning events in an urban atmosphere. In addition, it is also important to note that events identified using the TAP were a result of long-range atmospheric transport. These events were not detected using instrumentation located at the adjacent TCEQ CAMS 12 site.

In order to better distinguish dust and biomass burning events, a three-wavelength Nephelometer was co-located with the two TAP instruments. The utility of the co-located instrumentation (specifically the nephelometer) was assessed as part of this project. In this study, the SAE values calculated from the scattering coefficients, helped reduced the likelihood of a false positivity, specifically due to dust events. Evidence of this was during a known dust event (April 10th, 2019), where the SAE values decreased well below baseline (approaching 0), while the AAE increased to values similar to values associated with biomass-burning events. Data from this campaign suggests that the TAP in combination with a three-wavelength nephelometer is well-suited at identifying biomass-burning events in an urban landscape that is impacted by dust. El Paso, along with other major urban areas across Texas, has well documented history of dust events. Most notable, Houston has experienced periods of dust associated both with local roadways and long-range atmospheric transport of Saharan dust. It is also important to note, that other co-located instrumentation (such as CO) did not spike or peak during these events. This may be due to the magnitude of the biomass burning events identified

during the campaign as well as the relative background concentrations of CO and other trace gases in El Paso (i.e. an urban area with strong fossil fuel combustion sources).

The two TAP instruments had good comparability over the course of the campaign, which was achieved through optimization prior to deployment. The TAP has a small footprint (space, power, and volume) that could potentially be included at additional TCEQ monitoring sites. The TAPs and nephelometer were able to continuously measure aerosol optical properties during the campaign (>99%). The TAP is also being used by other groups including the National Oceanic and Atmospheric Administration, which developed the previous system called the continuous light absorption photometer.

7.0 Recommendations

This project investigated the ability of the TAP and nephelometer to identify influence biomass-burning events on El Paso air quality. Biomass-burning events identified were supported using remote sensing data, specifically satellite smoke and fire products and back trajectories. Since the NOAA hazard mapping for smoke does not indicate whether the plumes reach ground level, the TAP plus nephelometer combination does provide valuable information on whether smoke plumes impact the urban air quality or whether the smoke plumes have remained aloft. Based on the success of this project and the needs to identify influence of biomass-burning events in other cities, we recommend similar field campaigns and analysis to be conducted Houston, El Paso (as a continuation), and other cities in the State of Texas. In Houston, we also recommend the development of an optical network to examine the spatial extent and transport across the metropolitan area.

We also recommend using these systems as a real-time indicator of biomass-burning influence. Used in this way there is an opportunity to add additional measurements to bolster the optical measurements (e.g., filter-based potassium ion and radiocarbon) and improve quantification of the plume impacts. Combining results of biomass burning and dust identification through AAE and SAE with additional characterization could be used to potentially help understand the magnitude of event. Optical measurement can also be combined with real-time particle speciation (e.g. High-Resolution Time-of-Flight Aerosol Mass Spectrometer), aerosol optical depth measurements, and chemical transport modeling (e.g. GEOS-Chem) to fully characterize biomass burning events. With additional gas measurements

and modeling, it will be possible to improve understanding of the impact of biomass-burning events with ozone production.

8.0 References

Andreae, M. O., and A. Gelencser. 2006. Black carbon or brown carbon? The nature of light-absorbing carbonaceous aerosols. Atmospheric Chemistry and Physics **6**:3131-3148.

Bahadur, R., P. S. Praveen, Y. Y. Xu, and V. Ramanathan. 2012. Solar absorption by elemental and brown carbon determined from spectral observations. Proceedings of the National Academy of Sciences of the United States of America **109**:17366-17371.

Becerril-Valle, M., E. Coz, A. S. H. Prevot, G. Mocnik, S. N. Pandis, A. M. S. de la Campa, A. Alastuey, E. Diaz, R. M. Perez, and B. Artinano. 2017. Characterization of atmospheric black carbon and co-pollutants in urban and rural areas of Spain. Atmospheric Environment **169**:36-53.

Bond, T. C., T. L. Anderson, and D. Campbell. 1999. Calibration and intercomparison of filter-based measurements of visible light absorption by aerosols. Aerosol Science & Technology **30**:582-600.

Bond, T. C., and R. W. Bergstrom. 2006. Light absorption by carbonaceous particles: An investigative review. Aerosol Science and Technology **40**:27-67.

Briggs, N. L., and C. M. Long. 2016. Critical review of black carbon and elemental carbon source apportionment in Europe and the United States. Atmospheric Environment **144**:409-427.

Brown, S. G., T. Lee, P. T. Roberts, and J. L. Collett. 2016. Wintertime Residential Biomass Burning in Las Vegas, Nevada; Marker Components and Apportionment Methods. Atmosphere **7**.

Cappa, C. D., X. L. Zhang, L. M. Russell, S. Collier, A. K. Y. Lee, C. L. Chen, R. Betha, S. J. Chen, J. Liu, D. J. Price, K. J. Sanchez, G. R. McMeeking, L. R. Williams, T. B. Onasch, D. R. Worsnop, J. Abbatt, and Q. Zhang. 2019. Light Absorption by Ambient Black and Brown Carbon and its Dependence on Black Carbon Coating State for Two California, USA, Cities in Winter and Summer. Journal of Geophysical Research-Atmospheres **124**:1550-1577.

Chalbot, M.-C., I. G. Kavouras, and D. W. Dubois. 2013. Assessment of the contribution of wildfires to ozone concentrations in the central US-Mexico border region. Aerosol Air Qual. Res **13**:838-848.

Currie, J., E. A. Hanushek, E. M. Kahn, M. Neidell, and S. G. Rivkin. 2009. Does pollution increase school absences? The Review of Economics and Statistics **91**:682-694.

Dallmann, T. R., T. B. Onasch, T. W. Kirchstetter, D. R. Worton, E. C. Fortner, S. C. Herndon, E. C. Wood, J. P. Franklin, D. R. Worsnop, A. H. Goldstein, and R. A. Harley. 2014. Characterization of particulate matter emissions from on-road gasoline and diesel vehicles using a soot particle aerosol mass spectrometer. Atmospheric Chemistry and Physics **14**:7585-7599.

Garg, S., B. P. Chandra, V. Sinha, R. Sarda-Esteve, V. Gros, and B. Sinha. 2016. Limitation of the Use of the Absorption Angstrom Exponent for Source Apportionment of Equivalent

Black Carbon: a Case Study from the North West Indo-Gangetic Plain. Environmental Science & Technology **50**:814-824.

Healy, R. M., U. Sofowote, Y. Su, J. Debosz, M. Noble, C. H. Jeong, J. M. Wang, N. Hilker, G. J. Evans, G. Doerksen, K. Jones, and A. Munoz. 2017. Ambient measurements and source apportionment of fossil fuel and biomass burning black carbon in Ontario. Atmospheric Environment **161**:34-47.

Kirchstetter, T. W., C. V. Preble, O. L. Hadley, T. C. Bond, and J. S. Apte. 2017. Large reductions in urban black carbon concentrations in the United States between 1965 and 2000. Atmospheric Environment **151**:17-23.

Kondo, Y., H. Matsui, N. Moteki, L. Sahu, N. Takegawa, M. Kajino, Y. Zhao, M. J. Cubison, J. L. Jimenez, S. Vay, G. S. Diskin, B. Anderson, A. Wisthaler, T. Mikoviny, H. E. Fuelberg, D. R. Blake, G. Huey, A. J. Weinheimer, D. J. Knapp, and W. H. Brune. 2011. Emissions of black carbon, organic, and inorganic aerosols from biomass burning in North America and Asia in 2008. Journal of Geophysical Research-Atmospheres **116**.

Laing, J. R., D. A. Jaffe, and J. R. Hee. 2016. Physical and optical properties of aged biomass burning aerosol from wildfires in Siberia and the Western USA at the Mt. Bachelor Observatory. Atmos. Chem. Phys. **16**:15185-15197.

Lin, Y. H., H. Budisulistiorini, K. Chu, R. A. Siejack, H. F. Zhang, M. Riva, Z. F. Zhang, A. Gold, K. E. Kautzman, and J. D. Surratt. 2014. Light-Absorbing Oligomer Formation in Secondary Organic Aerosol from Reactive Uptake of Isoprene Epoxydiols. Environmental Science & Technology **48**:12012-12021.

Müller, T., J. S. Henzing, G. de Leeuw, A. Wiedensohler, A. Alastuey, H. Angelov, M. Bizjak, M. Collaud Coen, J. E. Engström, C. Gruening, R. Hillamo, A. Hoffer, K. Imre, P. Ivanow, G. Jennings, J. Y. Sun, N. Kalivitis, H. Karlsson, M. Komppula, P. Laj, S. M. Li, C. Lunder, A. Marinoni, S. Martins dos Santos, M. Moerman, A. Nowak, J. A. Ogren, A. Petzold, J. M. Pichon, S. Rodriquez, S. Sharma, P. J. Sheridan, K. Teinilä, T. Tuch, M. Viana, A. Virkkula, E. Weingartner, R. Wilhelm, and Y. Q. Wang. 2011. Characterization and intercomparison of aerosol absorption photometers: result of two intercomparison workshops. Atmos. Meas. Tech. **4**:245-268.

Ogren, J. A. 2010. Comment on Calibration and Intercomparison of Filter-Based Measurements of Visible Light Absorption by Aerosols. Aerosol science and technology **44**:589-591.

Ogren, J. A., J. Wendell, E. Andrews, and P. J. Sheridan. 2017. Continuous light absorption photometer for long-term studies. Atmos. Meas. Tech. **10**:4805-4818.

Ram, K., and M. M. Sarin. 2009. Absorption Coefficient and Site-Specific Mass Absorption Efficiency of Elemental Carbon in Aerosols over Urban, Rural, and High-Altitude Sites in India. Environmental Science & Technology **43**:8233-8239.

Ram, K., M. M. Sarin, and S. N. Tripathi. 2010. Inter-comparison of thermal and optical methods for determination of atmospheric black carbon and attenuation coefficient from an urban location in northern India. Atmospheric Research **97**:335-342.

Rolph, G., A. Stein, and B. Stunder. 2017. Real-time Environmental Applications and Display sYstem: READY. Environmental Modelling & Software **95**:210-228.

Sandradewi, J., A. S. Prévôt, S. Szidat, N. Perron, M. R. Alfarra, V. A. Lanz, E. Weingartner, and U. Baltensperger. 2008a. Using aerosol light absorption measurements for the quantitative determination of wood burning and traffic emission contributions to particulate matter. Environmental science & technology **42**:3316-3323.

Sandradewi, J., A. S. H. Prevot, S. Szidat, N. Perron, M. R. Alfarra, V. A. Lanz, E. Weingartner, and U. Baltensperger. 2008b. Using aerosol light absorption measurements for the quantitative determination of wood burning and traffic emission contributions to particulate matter. Environmental Science & Technology **42**:3316-3323.

Schmeisser, L., E. Andrews, J. A. Ogren, P. Sheridan, A. Jefferson, S. Sharma, J. E. Kim, J. P. Sherman, M. Sorribas, I. Kalapov, T. Arsov, C. Angelov, O. L. Mayol-Bracero, C. Labuschagne, S. W. Kim, A. Hoffer, N. H. Lin, H. P. Chia, M. Bergin, J. Sun, P. Liu, and H. Wu. 2017. Classifying aerosol type using in situ surface spectral aerosol optical properties. Atmos. Chem. Phys. **17**:12097-12120.

Schwarz, J. P., S. J. Doherty, F. Li, S. T. Ruggiero, C. E. Tanner, A. E. Perring, R. S. Gao, and D. W. Fahey. 2012. Assessing recent measurement techniques for quantifying black carbon concentration in snow. Atmos. Meas. Tech. Discuss. **5**:3771-3795.

Sinha, P. R., Y. Kondo, M. Koike, J. A. Ogren, A. Jefferson, T. E. Barrett, R. J. Sheesley, S. Ohata, N. Moteki, H. Coe, D. Liu, M. Irwin, P. Tunved, P. K. Quinn, and Y. Zhao. 2017. Evaluation of ground-based black carbon measurements by filter-based photometers at two Arctic sites. Journal of Geophysical Research-Atmospheres **122**:3544-3572.

Snyder, D. C., and J. J. Schauer. 2007. An inter-comparison of two black carbon aerosol instruments and a semi-continuous elemental carbon instrument in the urban environment. Aerosol science and technology **41**:463-474.

Stein, A. F., R. R. Draxler, G. D. Rolph, B. J. B. Stunder, M. D. Cohen, and F. Ngan. 2015. Noaa's Hysplit Atmospheric Transport and Dispersion Modeling System. Bulletin of the American Meteorological Society **96**:2059-2077.

Subramanian, R., G. L. Kok, D. Baumgardner, A. Clarke, Y. Shinozuka, T. L. Campos, C. G. Heizer, B. B. Stephens, B. de Foy, P. B. Voss, and R. A. Zaveri. 2010. Black carbon over Mexico: the effect of atmospheric transport on mixing state, mass absorption cross-section, and BC/CO ratios. Atmospheric Chemistry and Physics **10**:219-237.

Tasoglou, A., G. Saliba, R. Subramanian, and S. N. Pandis. 2017. Absorption of chemically aged biomass burning carbonaceous aerosol. Journal of Aerosol Science **113**:141-152.

Titos, G., A. del Águila, A. Cazorla, H. Lyamani, J. A. Casquero-Vera, C. Colombi, E. Cuccia, V. Gianelle, G. Močnik, A. Alastuey, F. J. Olmo, and L. Alados-Arboledas. 2017. Spatial and temporal variability of carbonaceous aerosols: Assessing the impact of biomass burning in the urban environment. Science of The Total Environment **578**:613-625.

Virkkula, A., N. C. Ahlquist, D. S. Covert, W. P. Arnott, P. J. Sheridan, P. K. Quinn, and D. J. Coffman. 2005. Modification, calibration and a field test of an instrument for measuring light absorption by particles. Aerosol science and technology **39**:68-83.

Wang, X., C. L. Heald, A. J. Sedlacek, S. S. de Sa, S. T. Martin, M. L. Alexander, T. B. Watson, A. C. Aiken, S. R. Springston, and P. Artaxo. 2016. Deriving brown carbon from multiwavelength absorption measurements: method and application to AERONET and Aethalometer observations. Atmospheric Chemistry and Physics **16**:12733-12752.

Washenfelder, R. A., A. R. Attwood, C. A. Brock, H. Guo, L. Xu, R. J. Weber, N. L. Ng, H. M. Allen, B. R. Ayres, K. Baumann, R. C. Cohen, D. C. Draper, K. C. Duffey, E. Edgerton, J. L. Fry, W. W. Hu, J. L. Jimenez, B. B. Palm, P. Romer, E. A. Stone, P. J. Wooldridge, and S. S. Brown. 2015. Biomass burning dominates brown carbon absorption in the rural southeastern United States. Geophysical Research Letters **42**:653-664.

Xie, M. J., X. Chen, M. D. Hays, M. Lewandowski, J. Offenberg, T. E. Kleindienst, and A. L. Holder. 2017. Light Absorption of Secondary Organic Aerosol: Composition and Contribution of Nitroaromatic Compounds. Environmental Science & Technology **51**:11607-11616.

Zhi, G. R., Y. J. Chen, Z. G. Xue, F. Meng, J. Cai, G. Y. Sheng, and J. M. Fu. 2014. Comparison of elemental and black carbon measurements during normal and heavy haze periods: implications for research. Environmental Monitoring and Assessment **186**:6097-6106.